Hf and Nd isotopes in Early Ordovician to Early Carboniferous granites as monitors of crustal growth in the Proto-Andean margin of Gondwana

Juan A. Dahlquist [a,b,*], Robert J. Pankhurst [c], Richard M. Gaschnig [d], Carlos W. Rapela [e], César Casquet [f], Pablo H. Alasino [b,g], Carmen Galindo [f], Edgardo G. Baldo [a]

[a] CICTERRA-CONICET-UNC, Av. Vélez Sarsfield 1611, Pab. Geol., X5016CGA, Córdoba, Argentina
[b] INGeReN-CENIIT-UNLaR. Av. Gob. Vernet y Apóstol Felipe. 5300, La Rioja, Argentina
[c] British Geological Survey, Keyworth, Nottingham NG12 5GG, UK
[d] Department of Geology University of Maryland College Park, MD 20742, USA
[e] CIG-CONICET-UNLP, Calle 1 Nº 644, 1900, La Plata, Argentina
[f] Departamento de Petrología y Geoquímica e Instituto de Geociencias, Universidad Complutense de Madrid-CSIC, Madrid 28040, Spain
[g] CRILAR-CONICET, Entre Ríos y Mendoza. 5301, Anillaco, La Rioja, Argentina

ARTICLE INFO

ABSTRACT

We report the first study integrating in situ U–Pb and Hf isotope data from magmatic zircon and whole-rock Sm–Nd isotope data for granitic rocks of the Sierras Pampeanas, Argentina, in order to evaluate the Palaeozoic growth of the proto-Andean margin of Gondwana. Early–Middle Ordovician granitic magmatism is by far the most voluminous of the Sierras Pampeanas and represents the most significant magmatic event. These calc-alkaline granitoids were intruded at an active continental margin. ε_{Hft} values range from -3.3 to -14.7 and ε_{Ndt} from -3.3 to -6.3 ($t = 473$ Ma), with average T_{DM} Hf and T_{DM} Nd ranging from 1.5 to 2.2 Ga and 1.4 to 1.7 Ga, respectively. Middle–Late Devonian magmatism occurred in the foreland, away from the orogenic front in the west, and included F-U-REE rich A-type granites. The Achala granite, the largest batholith in the Sierras Pampeanas, has ε_{Hft} and ε_{Ndt} values ranging from -3.6 to -5.8 and -4.0 to -6.5, respectively ($t = 369$ Ma). Small scattered Early Carboniferous A-type granite plutons were intruded in a dominantly extensional setting and have ε_{Hft} and ε_{Ndt} values ranging from -6.7 to $+2.2$ and -0.5 to -3.6, respectively ($t = 341$ Ma). The generation of Ordovician and Devonian magmas dominantly involved crustal reworking and stabilization rather than the formation of new continental crust by juvenile material accretion, whereas Carboniferous magmatism resulted in part from reworking of supracrustal material, but with variable addition of juvenile magmas.

© 2012 International Association for Gondwana Research. Published by Elsevier B.V. All rights reserved.

1. Introduction

As the pre-eminent U–Pb geochronometer, zircon plays a key role in crustal evolution studies. Recent analytical advances permit investigation of complex zircon grains at high spatial resolution, where the goal is to link U–Pb ages to other geochemical information, such as Hf isotopic composition. Thus zircon can provide time-stamped 'snapshots' of Hf isotope signatures of magmas throughout Earth's history, even at the scale of individual growth zones within a single grain. This information is an invaluable help to geochemists trying to distinguish magmatic events that added new mantle-derived material to the continental crust from those that recycled existing crust (e.g., Scherer et al., 2007; Siebel and Chen, 2010). Hence, during the last decade detrital zircon has been used intensively to study the mechanisms of growth and recycling of continental crust through time (Hawkesworth et al., 2010 and references therein).

Kemp et al. (2006) reported the first study combining hafnium and oxygen isotopes measured in situ on the same, precisely dated, detrital zircon grains. Their study of metasediments from the Ordovician accretionary system at the Pacific margin of eastern Australia showed that crustal growth was fundamentally episodic and confined to two major pulses at 1.9 and 3.3 Ga. In contrast, zircon crystallized corresponding to the most prominent detrital peaks at ca. 500 Ma registered magmatic episodes related to crustal reworking and stabilization, rather than the generation of new continental crust.

Until now the most commonly accepted idea for petrogenesis in the Gondwana margin magmatic arcs of the Sierras Pampeanas has been based on whole-rock Nd and Sr isotope data and involves a major contribution of crustal material in the Early Ordovician granites of the Famatinian belt (Pankhurst et al., 1998, 2000; Dahlquist et al., 2008) and a variable juvenile contribution during the A-type Carboniferous magmatism (Dahlquist et al., 2010; Alasino et al., 2012).

Recently, crustal evolution in the proto-Andean region was assessed by Willner et al. (2008) and Bahlburg et al. (2009) using data for detrital zircon in Late Paleozoic coastal accretionary systems

* Corresponding author at: CICTERRA-CONICET-UNC, Av. Vélez Sarsfield 1611, Pab. Geol., X5016CGA, Córdoba, Argentina. Tel.: +54 351 4344980; fax: +54 351 4334139.
E-mail address: jdahlquist@efn.uncor.edu (J.A. Dahlquist).

in central Chile and the Guarguaráz complex in Western Argentina (29°–36° L.S.). According to these authors the Famatinian granites were originated by recycling of mainly Mesoproterozoic crust. In contrast, zircons from Carboniferous igneous sources reflect either crustal contamination of juvenile parent magmas or, more likely, recycling of more juvenile crustal material (Willner et al., 2008).

In this article we report in situ U–Pb and Hf isotope data from zircons and whole-rock Sm/Nd data from Ordovician, Devonian, and Carboniferous host granites in order to evaluate their origin and so develop more detailed geodynamic models for the generation and evolution of the crust in the proto-Andean margin of Gondwana during the three main Palaeozoic magmatic events known in the Sierras Pampeanas of NW Argentina.

2. Regional setting

The proto-Andean margin of Gondwana is a good example of an accretionary orogen that has been active from at least the Early Ordovician to the present (Cawood, 2005), leading to the formation of different plutonic rocks during the Palaeozoic. Geochronological data and their interpretation in terms of major magmatic episodes allow the recognition of four main granitoid groups in the Eastern Sierras Pampeanas of NW Argentina (Fig. 1): Early Cambrian (Pampean), Early–Middle Ordovician (Famatinian), Middle–Late Devonian (Achalian) and Early Carboniferous. We have studied granitic rocks from the last three of these groups. Famatinian granitoids are typical calc-alkaline granites, formed in an active continental margin; those emplaced during the Achalian and Early Carboniferous events have dominantly A-type signatures.

The Famatinian arc (Fig. 1) is widely accepted to have been constructed on continental crust (Pankhurst et al., 1998; Rapela, 2000; Dahlquist and Galindo, 2004; Miller and Söllner, 2005; Dahlquist et al., 2008; Grosse et al., 2011). In the Famatinian magmatic belt of the Sierras Pampeanas, Pankhurst et al. (2000) identified three distinct granite-types: dominant I-type, S-type, and small-scale tonalite–trondhjemite–granodiorite (TTG) type (confined to the Sierras de Córdoba, see fig. 1 of Pankhurst et al., 2000). These three granite types can be distinguished petrologically, geochemically, and spatially, although all were emplaced within the 484–463 Ma interval (see also Dahlquist et al., 2008). Detailed petrological and geochemical studies of these rocks are given by Rapela et al. (1990), Aceñolaza et al. (1996), Saavedra et al. (1998), Pankhurst et al. (1998, 2000), Dahlquist and Galindo (2004), Miller and Söllner (2005), Dahlquist (2002), Dahlquist et al. (2005, 2007, 2008), Ducea et al. (2010), Grosse et al. (2011), and Otamendi et al. (2012).

The widespread Famatinian magmatism yielded extensive I-type intrusions (mostly tonalite, granodiorite and minor monzogranite and gabbro) with $\varepsilon_{Ndt} = -3$ to -6 (data from Pankhurst et al., 1998, 2000; Dahlquist and Galindo, 2004; Dahlquist et al., 2008; Grosse et al., 2011) and $\varepsilon_{Ndt} = -3$ to -9 for intermediate and felsic granitic units (Otamendi et al., 2012). Most of the gabbros in Sierra de Valle Fértil (Fig. 1) have negative ε_{Ndt} values ranging from -2.4 to -5.1. Only two analyzed gabbros reached more radiogenic values of ε_{Ndt} ($+0.25$ and $+0.9$, Otamendi et al., 2009, 2012), and subordinate small-scale isolated Ordovician plutons of Na-rich granite located in the Pampean belt foreland (TTG suites) have $\varepsilon_{Ndt} = +1.6$ to -0.2. Most of the Famatinian granitic rocks have T_{DM} model ages between 1.7 and 1.5 Ga (data from Pankhurst et al., 1998, 2000; Dahlquist and Galindo, 2004; Dahlquist et al., 2008) and Nd isotopic signatures suggesting derivation from a composite Palaeo-Mesoproterozoic lithospheric section that included lower and upper crustal sources as well as the sub-lithospheric mantle. Thus, it is usually argued that the Famatinian magmatic arc reworked old lithospheric sources, with little addition of juvenile material (Pankhurst et al., 2000; Dahlquist et al., 2008; Rapela et al., 2008a and references therein).

Dahlquist et al. (2008) concluded that: (i) the Famatinian magmatism was brief (~484 to ~463 Ma, see also Pankhurst et al., 2000), in contrast to the long-lived Mesozoic–Cenozoic cordilleran magmatism of the Andes; and (ii) the Early to mid-Ordovician development of ensialic marine basins was synchronous with the emplacement of voluminous lithosphere-derived magmatism in the central region of the Famatinian orogenic belt, in strong contrast with the Andean-type model for the production of magmas (Dahlquist and Galindo, 2004; Rapela et al., 2008a). This magmatism was completely extinguished during the mid-Ordovician and the marine sedimentary basins closed in the early Late Ordovician.

The Loma de las Chacras (Casquet et al., 2012) is a distinctive small circular outcrop that includes Ordovician felsic kyanite–garnet migmatite gneisses and garnet amphibolites, tectonically separated from the rest of the Sierra de Valle Fértil (Fig. 1). The amphibolites represent swarms of former dykes, some several meters thick, transported into parallelism with the foliation of the host migmatite. The Loma de Las Chacras amphibolites have positive ε_{Ndt} ranging from $+1.8$ to $+4.8$ (Casquet et al., 2012), suggesting a juvenile material contribution (see discussion in Section 6.1).

The ca. 2500 km² Achala batholith in the Sierras de Córdoba (Fig. 1) was emplaced during the upper Middle-to-Late Devonian: 368 ± 25 Ma U–Pb zircon, Dorais et al. (1997) and 379 ± 4 and 369 ± 3 Ma U–Pb SHRIMP zircon, Rapela et al. (2008b) (Fig. 1). It is the largest of a series of intrusive granitic bodies in the Sierras Pampeanas that are conspicuously discordant to structures and rocks formed during the Cambrian (Pampean) and Ordovician (Famatinian) metamorphic events. Contact aureoles indicate shallow emplacement, usually less than 2 kbar (e.g., Baldo, 1992; Pinotti et al., 2002). Rapela et al. (2008b) concluded that the Achala batholith has an A-type signature. Sims et al. (1998), Stuart-Smith et al. (1999), and Siegesmund et al. (2004) considered the voluminous Devonian intrusive rocks in the Sierras de Córdoba and the eastern area of the Sierras de San Luis to have been emplaced during compression associated with Late Devonian low-grade shear zones, together defining the Achalian orogeny (Middle-to-Late Devonian). According to this interpretation the Devonian granites, such as the Achala (Sims et al., 1998) and Cerro Áspero batholiths in Sierra de Córdoba (e.g., Pinotti et al., 2002, 2006), and the Las Chacras (Siegesmund et al., 2004) and Renca (Stuart-Smith et al., 1999) batholiths in Sierra de San Luis (Fig. 1), are not post-orogenic intrusions of the Famatinian Orogeny as proposed by Pankhurst and Rapela (1998), but belong to a distinct tectonomagmatic event. The Late Devonian compressional event is controversial and has been related to: (i) collision of the suggested Chilenia terrane with the proto-Pacific margin (Willner et al., 2011), (ii) final collision between the Famatinian magmatic arc and the Pampean hinterland (Höckenreiner et al., 2003) and, recently, (iii) push–pull tectonic switching episodes during Devonian and Carboniferous time, resulting from flat-slab/roll-back subduction along the Pacific margin (Alasino et al., 2012). The A-type geochemical signature of the Achala batholith (Rapela et al., 2008b) strongly suggests intracratonic magmatism in a dominantly extensional regime with subsequent lithospheric thinning (Early–Middle Devonian?), followed by Late Devonian horizontal shortening and Early Carboniferous lithospheric stretching (see tectonic switching model of Collins, 2002).

In Carboniferous times, isolated and dispersed granitic plutons with anorogenic signatures were emplaced along more than 1000 km in the Sierras Pampeanas of NW Argentina (see Dahlquist et al., 2010, fig. 1). They are represented by small and scattered plutons, usually subcircular, intruded mainly along prominent shear zones (Dahlquist et al., 2010). Host rocks to this Carboniferous magmatism were formed during three main periods of magmatic and metamorphic activity: Middle Cambrian (Pampean orogeny), Early–Middle Ordovician (Famatinian orogeny), and Middle–Late Devonian (Achalian event) (Pankhurst et al., 1998, 2000; Sims et al., 1998; Dahlquist et al., 2008;
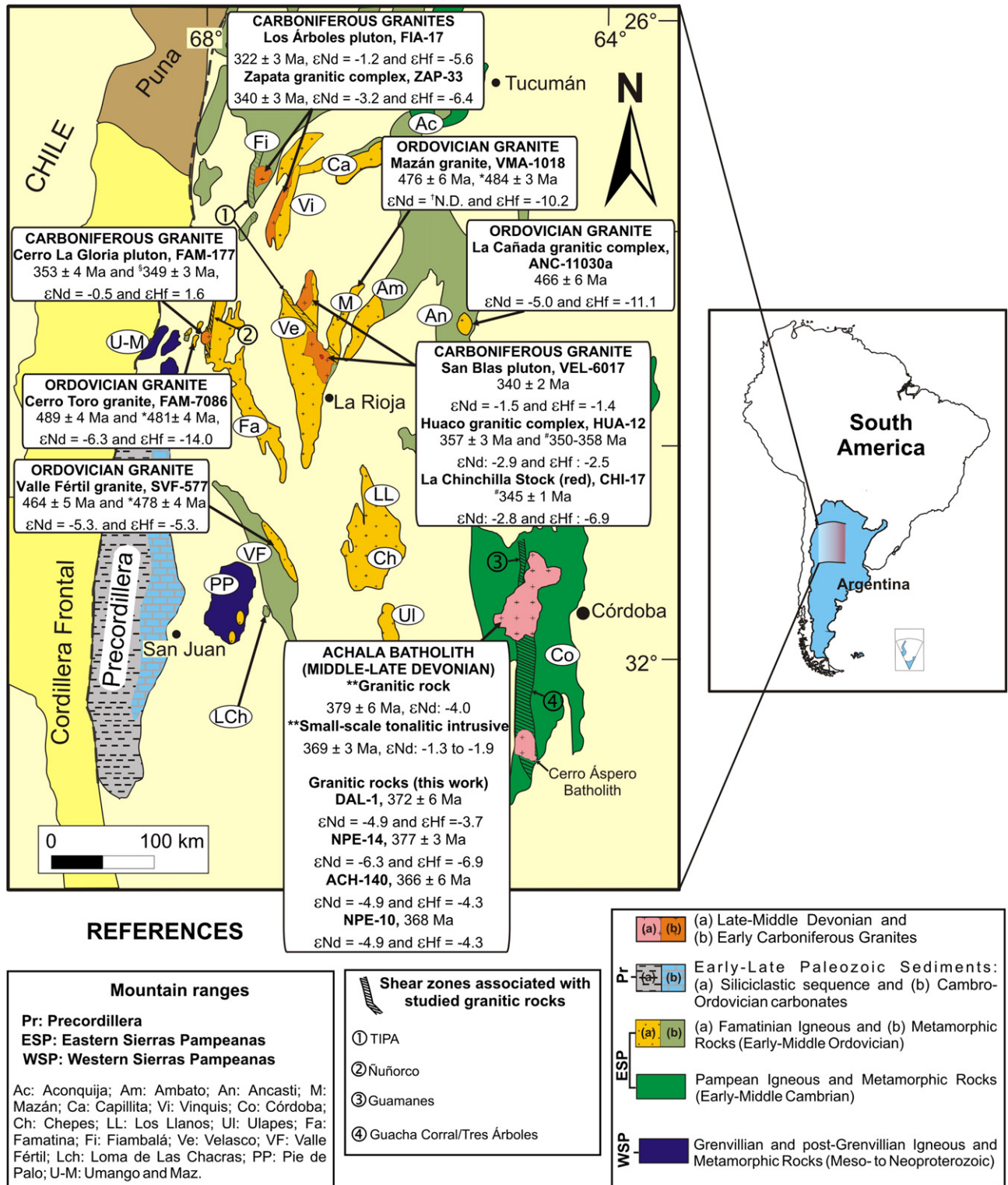
Fig. 1. Simplified geological map of central-west Argentina (Sierras Pampeanas), central Chile, and the location of the studied Early–Middle Ordovician calc-alkaline granites and Middle–Late Devonian (Achala batholith) and Early Carboniferous A-type granites. The La Chinchilla stock outcrop is magnified so that it can be seen (for details see Grosse et al., 2009; fig. 1). Coupled in situ U–Pb ages and Hf isotope data for zircons and whole-rock Sm/Nd data are included. Sources: *U–Pb zircon SHRIMP (Pankhurst et al., 2000); #U–Pb monazite TIMS (Grosse et al., 2009); †N.D. = not determined; §U–Pb zircon SHRIMP (Alasino et al., 2012); **U–Pb zircon SHRIMP (Rapela et al., 2008b), otherwise data reported in this paper. Inset: schematic map of South America showing the location of Sierras Pampeanas in Argentina.

Rapela et al., 2008a, 2008b; Vaughan and Pankhurst, 2008; Alasino et al., 2012; Spagnuolo et al., 2012; Tohver et al., 2012).

The geodynamic setting of the Carboniferous magmatism remains controversial. Some authors have suggested that it resulted from crustal reheating as the final phase of a protracted Famatinian orogeny

extending from the Ordovician to Early Carboniferous (e.g., Grissom et al., 1998; Llambías et al., 1998; Höckenreiner et al., 2003; Grosse et al., 2009). Others have argued for a distinctive and extended Achalian orogenic event in the Devonian–Early Carboniferous (e.g., Sims et al., 1998; Stuart-Smith et al., 1999; López de Luchi et al., 2004; Siegesmund et al.,

Table 1
Integrated in situ U–Pb and Hf isotopes in zircon and whole-rock and isotopes data for the studied rocks (see Fig. 1).

	U–Pb ages[a]	U–Pb ages[b]	εNd (t)[c]	εHf (t)	T_{DM} Nd	T_{DM} Hf	Latitude	Longitude
Early–Middle Ordovician granitic rocks								
Samples								
SVF-577 (Sierra de Valle Fértil)	464 ± 5	478 ± 4	−5.4	−5.7	1.6	1.7	30° 39′ 28″	67° 36′ 17″
VMA-1018 (Sierra de Mazán)	476 ± 6	484 ± 3	N.D.[d]	−7.3	N.D.	1.8	28° 43′ 31″	66° 34′ 31″
FAM-7086 (Sierra de Famatina)	483 ± 8	481 ± 4	−5.9	−14.7	1.7	2.2	29° 01′ 25″	68° 10′ 19″
ANC-11030a (Sierra de Ancasti)	466 ± 6	N.D.	−4.9	−3.3	1.6	1.5	28° 57′ 56″	65° 25′ 08″
Middle–Late Devonian granitic rocks								
ACH-140 (Batolito de Achala)	366 ± 6	N.D.	−5.0	−3.8	1.5	1.5	31° 36′ 37″	64° 49′ 49″
DAL-1 (Batolito de Achala)	372 ± 6	N.D.	−4.9	−3.6	1.5	1.5	31° 25′ 50″	64° 53′ 00″
NPE-14 (Batolito de Achala)	369 ± 5	N.D.	−6.3	−5.9	1.6	1.6	31° 26′ 02″	64° 49′ 29″
NPE-10 (Batolito de Achala)	369[e]	N.D.	−5.7	−3.8	1.6	1.5	31° 25′ 46″	64° 49′ 50″
Early Carboniferous granitic rocks								
FIA-17 (Los Árboles pluton)	322 ± 3	N.D.	−1.6	−5.0	1.2	1.6	27° 44′ 31″	67° 30′ 04″
VEL-6017 (San Blas pluton)	340 ± 2	340 ± 3	−1.6	−5.2 and +0.5	1.2	1.6 and 1.3	28° 27′ 14″	67° 06′ 02″
ZAP-33 (Zapata granitic complex)	332 ± 3	N.D.	−3.6	−5.8	1.4	1.6	27° 53′ 18″	67° 21′ 15″
FAM-177 (Cerro La Gloria pluton)	353 ± 4	349 ± 3[f]	−0.5	2.6	1.2	1.1	29°04′57.1″	67°57′03.9″
HUA-12 (Huaco granitic complex)	357 ± 3	N.D.	−2.9	−3.3	1.3	1.5	29° 11′ 23″	67° 01′ 45″
CHI-17 (La Chinchilla stock)	345 ± 1[g]	N.D.	−2.8	−6.7	1.3	1.7	29° 10′ 09″	66° 58′ 20″

Note: compilation of data from Tables 2 and 3. VMA-1018 is not available for Sm/Nd determinations. VEL-6017 defines two Hf compositions populations (see Table 2).

[a] U–Pb zircon LA-ICP-MS, this work.
[b] U–Pb zircon SHRIMP (Pankhurst et al., 2000; Dahlquist et al., 2008).
[c] t = 473, data from Table 3.
[d] N.D. = not determined.
[e] Average from ACH-140, DAL-1, and NPE-14. An U–Pb zircon age = 368 Ma was obtained by Dorais et al. (1997) for a rock such as NPE-10.
[f] U–Pb zircon SHRIMP from Alasino et al. (2012).
[g] U–Pb monazite LA-ICP-MS from Grosse et al. (2009).

2004; Dahlquist et al., 2006; Rapela et al., 2008b). Recently, Dahlquist et al. (2010) claimed that the Early Carboniferous A-type granites of the Eastern Sierras Pampeanas represent a tectonothermal event distinct from both Famatinian and Achalian magmatism. Field and geochemical data for this particular granite group are indicative of a distinctive extensional within-plate magmatic setting where compressive tectonic activity is absent (Dahlquist et al., 2010).

In summary, Devonian and Carboniferous magmatism would have been developed in an intracratonic orogen related to continental margin subduction according to the definition of Cawood et al. (2009). Current interpretations (e.g., Alasino et al., 2012) suggest that both magmatic events were linked to tectonic switching episodes on an active Pacific margin.

3. Analytical methods

3.1. Geochronology

Samples chosen for U–Pb zircon geochronology were prepared and analyzed at the School of Earth and Environmental Sciences (SEES), Washington State University (WSU). Samples were crushed and pulverized using a jaw crusher and disk mill followed by heavy mineral concentration using a Gemini table. Additional density separation was carried out using methylene iodide and magnetic separation using a Franz magnetic separator. Zircons (>90% pure) were mounted in epoxy within 2.5 cm diameter rings, polished to expose zircon interiors, and imaged with a Scanning Electron Microscope in cathode-luminescence (CL) mode at the University of Idaho.

All LA-ICP-MS U–Pb analyses were conducted at Washington State University using a New Wave Nd:YAG UV 213-nm laser coupled to a ThermoFinnigan Element 2 single collector, double-focusing, magnetic sector ICP-MS. Operating procedures and parameters are discussed in greater depth by Chang et al. (2006) and Gaschnig et al. (2010) and are only briefly outlined here. Laser spot size and repetition rate were 30 μm and 10 Hz, respectively. He and Ar carrier gases delivered the sample aerosol to the plasma. Time-independent (or static) fractionation is the largest source of uncertainty in LA-ICP-MS U–Pb

geochronology and results from mass and elemental static fractionation in the plasma and also poorly understood laser-matrix effects (Kosler and Sylvester, 2003). It is corrected by normalizing U/Pb and Pb/Pb ratios of the unknowns to the zircon standards (Chang et al., 2006). For this study we used two zircon standards: Peixe, with an age of 564 Ma (Dickinson and Gehrels, 2003), and FC-1, with an age of 1099 Ma (Paces and Miller, 1993).

Results are summarized in Table 1 and full data are given in Supplementary Table 1.

3.2. Hf isotope analysis

In-situ LA-MC-ICP-MS Hf isotope analyses were conducted at WSU using a New Wave 213 nm UP Nd:YAG laser coupled to a Thermo-Finnigan Neptune MC-ICP-MS with 9 Faraday collectors. The laser was operated at a pulse rate of 10 Hz and power density of 10–12 J/cm^2 with a spot size of 40 μm, except in a few cases where smaller grains and narrower zones required a smaller spot size of 30 μm. The carrier gas consisted of purified He with small quantities of N_2 to minimize oxide formation and increase sensitivity. Analyses consisted of 60 one-second measurements in static mode.

The greatest obstacle in LA-MC-ICP-MS Hf isotopic analysis is the isobaric interference of ^{176}Yb and ^{176}Lu on ^{176}Hf (e.g., Woodhead et al., 2004). Despite the extremely low Lu/Hf in zircon, ^{176}Yb can comprise more than 10% of the total signal at mass 176 and provides the largest source of uncertainty in the measurement. A partly empirical approach was used to correct for the Yb interference, in which a modified Yb isotopic composition was calculated with Yb mass bias determined by the relationship $\beta_{Yb} = x * \beta_{Hf}$. The value for x was determined by analyzing the zircon standards 91500, FC1, Peixe, GJ1, Mudtank, R33, Pleisovice, QGNG, and Temora and adjusting the x value to best fit the known ^{176}Hf/^{177}Hf values previously determined on chemically purified solutions. The x value and modified ^{176}Yb/^{173}Yb were then used to calculate the Hf isotopic composition of the unknowns.

Due to the difficulty in correcting for the Yb interference and other sources of error such as instrumental bias and matrix effects, the internal measurement error by itself is often considerably less than the total uncertainty, which is often difficult to estimate. Based on the deviation of $^{176}Hf/^{177}Hf$ values determined by the in situ method on the standards from the values determined by solution analysis, the total uncertainty for individual analyses is approximately ± 3σ units.

Present day and initial ε_{Hf} values were calculated using CHUR compositions of $^{176}Hf/^{177}Hf_{today} = 0.282785$ and $^{176}Lu/^{177}Hf = 0.0336$ (Bouvier et al., 2008) and a ^{176}Lu decay constant of $1.867e^{-11}$ (Söderlund et al., 2004; Scherer et al., 2007). The initial $^{176}Hf/^{177}Hf$ values at the time of zircon crystallization were used to calculate the hypothetical present-day $^{176}Hf/^{177}Hf$ of the zircons' parent rock based on an average crustal $^{176}Lu/^{177}Hf$ of 0.015 (Goodge and Vervoort, 2006). The present day $^{176}Hf/^{177}Hf$ and assumed rock $^{176}Lu/^{177}Hf$ values were then used to calculate a traditional T_{DM} using the equation: $(1/\lambda)*ln[(^{176}Hf/^{177}Hf \text{ (sample)} - ^{176}Hf/^{177}Hf \text{ (DM)})/(^{176}Lu/^{177}Hf \text{ (average crust)} - ^{176}Lu/^{177}Hf \text{ (DM)})]$. For the depleted mantle parameters, $^{176}Hf/^{177}Hf$ (DM) = 0.283225 and $^{176}Lu/^{177}Hf$ (DM) = 0.038512 (Vervoort and Blichert-Toft, 1999). Results are summarized in Table 1 and full data are given in Table 2 and Supplementary Table 2.

3.3. Sm–Nd isotope analysis

Sm–Nd determinations of representative dated granitic samples with Hf isotope zircon data were carried out at Washington State University. For Nd whole-rock isotopic analyses, ~0.25 g aliquots of whole-rock powders were dissolved at high pressure in sealed, steel-jacketed Teflon bombs with a 10:1 mixture of concentrated HF and HNO_3 acids at 150 °C for 5 to 7 days. After conversion from fluorides to chlorides, samples were spiked with a mixed $^{149}Sm–^{150}Nd$ tracer. LREE were initially separated on cation exchange columns using AG 50W-X8 (200–400 mesh) resins; Nd and Sm were then separated from the LREE aliquot on columns with HDEHP-coated Teflon powder and HCl (Vervoort and Blichert-Toft, 1999).

All analyses were conducted on a Thermo-Finnigan Neptune MC-ICP-MS. Nd and Sm analyses were corrected for mass fractionation by exponential law using $^{146}Nd/^{144}Nd = 0.7219$ and $^{147}Sm/^{152}Sm = 0.56081$, respectively. Nd analyses were normalized to the Ames and La Jolla Nd standards.

The uncertainties on Nd isotopic measurements reflect in-run error only and are presented as two standard errors as reported by Bouvier et al. (2008, table 2). The full uncertainties are better assessed from the reproducibility of the standards. Average reproducibility (2 standard deviations) of $^{143}Nd/^{144}Nd$ on the Ames standard during the period of analysis was ± 0.000020.

The decay constants used in the calculations are the values $\lambda^{147}Sm = 6.54 \times 10^{-12}$ year^{-1} recommended by the IUGS Subcommission for Geochronology (Steiger and Jäger, 1977). Epsilon-Nd (εNd) values were calculated relative to a CHUR: $(^{143}Nd/^{144}Nd)_{today}CHUR = 0.512638$; $(^{143}Sm/^{144}Nd)_{today}CHUR = 0.1967$ (Jacobsen and Wasserburg, 1980; Goldstein et al., 1984). T_{DM} was calculated according to DePaolo et al. (1991).

The results are reported in Table 3, together with published (and in some cases recalculated) data for other samples selected for Nd isotope analysis, as well as representative equivalent samples from the same igneous bodies.

3.4. Geochemistry

Whole-rock major elements were determined for three igneous samples at the Washington State University GeoAnalytical Lab, using a ThermoARL sequential X-ray fluorescence spectrometer, following the procedure described by Johnson et al. (1999). Trace elements were determined in the same samples using ICP-MS, following the procedure described in http://www.sees.wsu.edu/Geolab/note/icpms.html.

Additionally, whole-rock major and trace element compositions for two samples were determined at Activation Laboratories, Ontario, Canada (ACTLABS), following the 4-Lithoresearch procedure. Following lithium metaborate/tetraborate fusion, samples are dissolved in a weak nitric acid solution. Major elements, Be, Sc, V, Sr, Ba, and Zr are determined by Inductively Couple Plasma–Optical Emission Spectroscopy (ICP–OES). All other trace elements are determined by Inductively Coupled Plasma–Mass Spectrometry (ICP–MS). For major elements, precision and accuracy are generally better than 2% (relative). For trace elements, precision and accuracy are generally better than ± 6% for all elements determined at 10 times above background. Full data are given in Supplementary Table 3.

4. U–Pb geochronology

We investigated granitic rock samples that could be clearly assigned to each of the three age groups (i.e., Early–Middle Ordovician, Middle–Late Devonian, and Early Carboniferous), based on previously published SHRIMP U–Pb zircon age data. New U–Pb zircon ages were determined using LA-ICP-MS measured in situ on the same, precisely dated magmatic zircon grains. In a few cases LA-ICP-MS dating was carried out on zircon concentrates already analyzed by SHRIMP; these resulted in ages that agreed within statistical uncertainties. Our new U–Pb zircon LA-ICP-MS ages from granitic rocks of the Achala batholith also confirm the Middle–Late Devonian ages previously reported for other granitic rocks of this batholith (Dorais et al., 1997; Rapela et al., 2008b). For the Zapata granitic complex only K–Ar ages on biotite were available (323–316 Ma; McBride, 1972; McBride et al., 1976); our new U–Pb zircon LA-ICP-MS data indicate a crystallization age of 340 ± 2 Ma.

Sample locations as well as the ages are summarized in Table 1 and Fig. 1. Full geochronological data including U–Pb zircon Laser Inductively Coupled Plasma-Mass Spectrometry (LA-ICP-MS) ages of 12 granitic rocks are found in Supplementary Table 1.

5. Hf in zircon and whole-rock Nd isotope data

5.1. General considerations

Hf isotopes were determined from the magmatic growth rim zone of 14 zircons (Table 2, Supplementary Table 2 and summarized in Table 1), each of which had been first dated by LA-ICP-MS U–Pb isotope analysis (Supplementary Table 1). Only zircon areas shown to have crystallized during the primary magmatic event were analyzed for Hf isotopes. Inherited core zircon ages in Famatinian granitic rocks define mainly Mesoproterozoic–early Neoproterozoic (ca. 1150–850 Ma) and Neoproterozoic–early Cambrian (ca. 720–530 Ma) populations (data from Ducea et al., 2010), and inherited zircons with Ordovician ages have been reported from Carboniferous plutons by Grosse et al. (2009) and Fogliata et al. (2012). Whole-rock chemistry of the rocks with Hf and Nd isotope data is reported in Supplementary Table 3. Chemical data are not discussed here, but they are included as complementary information for those rocks with Hf and Nd isotope data.

The ε_{Hft} values for magmatic zircons are plotted as a function of the corresponding whole-rock Nd isotope composition at the time of crystallization (ε_{Ndt}) and also as a function of crystallization age (Tables 2, 3 and Fig. 2). As in the general study reported by Kemp et al. (2007), an important feature of the Hf isotope data is the significant range of ε_{Hft} values exhibited by zircons within the same sample (up to 10 ε units). Large scatter of the Hf isotope is well known because zircon can crystallize sufficiently early and retain vestiges of the original Hf isotope signature (Kemp et al., 2007). Such variations can be reconciled by changing the $^{176}Hf/^{177}Hf$ ratio of the

Table 2
Laser ablation Hf isotope data for igneous dated zircons from Sierras Pampeanas of Argentina (location of samples in Fig. 1 and Table 1).

Sample	Grain	Age (Ma)	$^{176}Hf/^{177}Hf$	±(2σ)	$^{176}Lu/^{177}Hf$	±(2σ)	$^{176}Yb/^{177}Hf$	Age (Ma)	εHf(today)	±(2σ)	εHf (t)	T_DM Hf
Early–Middle Ordovician granitic rocks (Ancasti, Famatina, Valle Fértil, and Mazán mountain ranges)												
ANC-11030a	4/3[a]											
	ANC-11030a_8a	466	0.282464	0.000062	0.001761	0.000100	0.068127	466	−11.4	2.2	−1.5	1.5
	ANC-11030a_3a	466	0.282386	0.000041	0.002333	0.000113	0.080279	466	−14.1	1.4	−4.5	1.6
	ANC-11030a_2a	466	0.282396	0.000039	0.001887	0.000120	0.075972	466	−13.7	1.4	−4.0	1.7
Average											−3.3	1.5
FAM-7086	8/5											
	FAM-7086_1b	489	0.282198	0.000043	0.002483	0.000073	0.076713	489	−20.8	1.5	−10.7	2.0
	FAM-7086_5a	489	0.282110	0.000035	0.002693	0.000144	0.088002	489	−23.9	1.3	−13.9	2.2
	FAM-7086_3a	489	0.281986	0.000030	0.004196	0.000377	0.119129	481	−28.3	1.1	−18.9	2.5
	FAM-7086_4a	489	0.282055	0.000065	0.002380	0.000074	0.072752	489	−25.8	2.3	−15.7	2.3
	FAM-7086_2b	489	0.282173	0.000037	0.002643	0.000108	0.085036	489	−21.6	1.3	−11.6	2.0
Average											−14.2	2.2
SVF-577	13/11											
	SVF-577_17a	464	0.282324	0.000061	0.000581	0.000013	0.025969	464	−16.3	2.2	−6.1	1.7
	SVF-577_15a	464	0.282375	0.000057	0.000902	0.000040	0.037338	464	−14.5	2.0	−4.5	1.6
	SVF-577_13a	464	0.282301	0.000046	0.000466	0.000016	0.020208	464	−17.1	1.6	−6.9	1.8
	SVF-577_11a	464	0.282335	0.000036	0.000260	0.000008	0.009712	464	−15.9	1.3	−5.7	1.7
	SVF-577_10a	464	0.282366	0.000046	0.000595	0.000037	0.020873	464	−14.8	1.6	−4.7	1.6
	SVF-577_8a	464	0.282334	0.000063	0.000434	0.000035	0.016921	464	−16.0	2.2	−5.8	1.7
	SVF-577_7a	464	0.282365	0.000067	0.000538	0.000037	0.021245	464	−14.9	2.4	−4.7	1.6
	SVF-577_6a	464	0.282380	0.000043	0.000445	0.000022	0.017711	464	−14.3	1.5	−4.1	1.6
	SVF-577_1a	464	0.282247	0.000059	0.000375	0.000019	0.011942	464	−19.0	2.1	−8.8	1.9
Average											−5.7	1.7
VMA-1018	8/8											
	VMA-1018_9a	476	0.282248	0.000032	0.001231	0.000083	0.056862	476	−19.0	1.1	−8.8	1.9
	VMA-1018_8a	476	0.282324	0.000030	0.002385	0.000276	0.121735	476	−16.3	1.1	−6.4	1.7
	VMA-1018_7a	476	0.282282	0.000034	0.003245	0.000219	0.147306	476	−17.8	1.2	−8.2	1.8
	VMA-1018_6a	476	0.282302	0.000044	0.003756	0.000648	0.145780	476	−17.1	1.6	−7.7	1.8
	VMA-1018_5a	476	0.282283	0.000035	0.001581	0.000157	0.066127	476	−17.8	1.2	−7.7	1.8
	VMA-1018_4a	476	0.282349	0.000021	0.001904	0.000171	0.095304	476	−15.4	0.8	−5.4	1.7
	VMA-1018_3a	476	0.282253	0.000030	0.002041	0.000031	0.093116	476	−18.8	1.2	−8.9	1.9
	VMA-1018_1a	476	0.282356	0.000042	0.001854	0.000089	0.091752	476	−15.2	1.5	−5.2	1.7
Average											−7.3	1.8
Late–Middle Devonian granitic rocks (Achala batholith)												
DAL-1	7/7											
	Dal-1_8a	372	0.282372	0.000062	0.000822	0.000032	0.038368	372	−14.6	2.2	−6.5	1.8
	Dal-1_7a	372	0.282462	0.000032	0.000659	0.000008	0.031781	372	−11.4	1.1	−3.3	1.6
	Dal-1_6a	372	0.282427	0.000045	0.000721	0.000045	0.033232	372	−12.7	1.6	−4.7	1.6
	Dal-1_4a	372	0.282482	0.000060	0.000756	0.000009	0.037214	372	−10.7	2.1	−2.6	1.4
	Dal-1_3a	372	0.282475	0.000033	0.000793	0.000018	0.037658	372	−11.0	1.2	−2.9	1.5
	Dal-1_2a	372	0.282498	0.000039	0.000586	0.000021	0.028253	372	−10.1	1.4	−2.0	1.4
	Dal-1_1a	372	0.282454	0.000028	0.000591	0.000009	0.027818	372	−11.7	1.0	−3.7	1.5
Average											−3.6	1.5
NPE-14	7/7											
	NPE-14_3c	369	0.282424	0.000042	0.000790	0.000021	0.041036	369	−12.8	1.5	−4.7	1.6
	NPE-14_3b	369	0.282449	0.000046	0.000779	0.000060	0.039925	369	−11.9	1.6	−3.8	1.5
	NPE-14_3a	369	0.282312	0.000049	0.001181	0.000144	0.048790	369	−16.7	1.7	−8.7	1.8
	NPE-14_2d	369	0.282373	0.000048	0.000691	0.000048	0.035585	369	−14.6	1.7	−6.5	1.7
	NPE-14_2c	369	0.282383	0.000052	0.000682	0.000043	0.034580	369	−14.2	1.9	−6.1	1.7
	NPE-14_2b	369	0.282415	0.000049	0.000708	0.000053	0.036478	369	−13.1	1.7	−5.0	1.6
	NPE-14_2a	369	0.282367	0.000045	0.000895	0.000050	0.037973	369	−14.8	1.6	−6.7	1.7
Average											−5.9	1.6
ACH-140	10/7											
	ACH-140_10a	366	0.282484	0.000023	0.000978	0.000051	0.051003	366	−10.6	0.8	−2.7	1.4
	ACH-140_9a	366	0.282468	0.000031	0.001216	0.000036	0.061520	366	−11.2	1.1	−3.4	1.5
	ACH-140_8a	366	0.282380	0.000050	0.001339	0.000183	0.055740	366	−14.3	1.8	−6.5	1.7
	ACH-140_6a	366	0.282480	0.000030	0.000836	0.000031	0.043617	366	−10.8	1.1	−2.8	1.4
	ACH-140_5a	366	0.282454	0.000025	0.000891	0.000017	0.044674	366	−11.7	0.9	−3.8	1.5
	ACH-140_2b	366	0.282434	0.000028	0.000893	0.000074	0.048033	366	−12.4	1.0	−4.5	1.5
	ACH-140_1a	366	0.282477	0.000025	0.000921	0.000061	0.048627	366	−10.9	0.9	−3.0	1.5
Average											−3.8	1.5
NPE-10	10/9											
	NPE-10_7a	369	0.282485	0.000033	0.000892	0.000032	0.042838	369	−10.6	1.2	−2.6	1.4
	NPE-10_6a	369	0.282371	0.000048	0.000794	0.000048	0.034683	369	−14.6	1.7	−6.6	1.7
	NPE-10_5a	369	0.282423	0.000030	0.001099	0.000069	0.048549	369	−12.8	1.1	−4.9	1.6
	NPE-10_4a	369	0.282447	0.000036	0.000850	0.000020	0.039005	369	−11.9	1.3	−3.9	1.5
	NPE-10_3b	369	0.282493	0.000033	0.000628	0.000051	0.031648	369	−10.3	1.2	−2.3	1.4
	NPE-10_2a	369	0.282464	0.000025	0.001387	0.000056	0.066827	369	−11.3	0.9	−3.5	1.5
	NPE-10_1c	369	0.282453	0.000043	0.001146	0.000016	0.048249	369	−11.7	1.5	−3.8	1.5
	NPE-10_1b	369	0.282500	0.000036	0.000997	0.000013	0.048892	369	−10.1	1.3	−2.1	1.4
	NPE-10_1a	369	0.282475	0.000049	0.000873	0.000033	0.040185	369	−11.0	1.8	−3.0	1.5
Average											−3.6	1.5

Table 2 (*continued*)

Sample	Grain	Age (Ma)	$^{176}Hf/^{177}Hf$	±(2σ)	$^{176}Lu/^{177}Hf$	±(2σ)	$^{176}Yb/^{177}Hf$	Age (Ma)	εHf$_{(today)}$	±(2σ)	εHf (t)	T$_{DM}$ Hf
Early Carboniferous granitic rocks (Fiambalá, Velasco, Famatina and Zapata mountain ranges).												
FIA-17	8/6											
	FIA-17_6b	322	0.282477	0.000074	0.000544	0.000002	0.026722	322	−10.9	2.6	−3.9	1.5
	FIA-17_4a	322	0.282493	0.000046	0.001762	0.000147	0.097517	322	−10.3	1.6	−3.5	1.4
	FIA-17_3b	322	0.282432	0.000067	0.000916	0.000027	0.045564	322	−12.5	2.4	−5.5	1.6
	FIA-17_3a	322	0.282359	0.000068	0.000627	0.000019	0.030277	322	−15.1	2.4	−8.0	1.7
	FIA-17_1b	322	0.282469	0.000064	0.000677	0.000011	0.034428	322	−11.2	2.3	−4.2	1.5
	FIA-17_1a	322	0.282445	0.000061	0.000557	0.000014	0.027907	322	−12.0	2.16	−5.0	1.6
Average											−5.0	1.6
HUA-12	7/5											
	HUA-12_6a	357	0.282523	0.000029	0.001206	0.000169	0.059043	357	−9.3	1.0	−1.6	1.4
	HUA-12_5b	357	0.282503	0.000051	0.001274	0.000072	0.065866	357	−10.0	1.8	−2.4	1.4
	HUA-12_4a	357	0.282471	0.000040	0.000989	0.000011	0.049964	357	−11.1	1.4	−3.4	1.5
	HUA-12_3a	357	0.282405	0.000038	0.001637	0.000033	0.084079	357	−13.4	1.3	−5.9	1.6
	HUA-12_1a	357	0.282469	0.000059	0.000771	0.000044	0.041285	357	−11.2	2.1	−3.4	1.5
Average											−3.3	1.5
CHI-17	3/3											
	CHI-7_5a	345	0.282363	0.000051	0.001324	0.000140	0.052209	345	−14.9	1.8	−7.6	1.7
	CHI-7_4a	345	0.282361	0.000032	0.001481	0.000235	0.062902	345	−15.0	1.1	−7.7	1.7
	CHI-7_2a	345	0.282440	0.000028	0.001475	0.000214	0.061438	345	−12.2	1.0	−4.9	1.5
Average											−6.7	1.7
FAM-177	11/9											
	FAM-177_3b	353	0.282605	0.000055	0.001347	0.000027	0.063763	353	−6.4	2.0	1.2	1.2
	FAM-177_6b	353	0.282666	0.000037	0.002280	0.000232	0.098271	353	−4.2	1.3	3.1	1.0
	FAM-177_5b	353	0.282655	0.000040	0.001772	0.000030	0.088599	353	−4.6	1.4	2.8	1.1
	FAM-177_4b	353	0.282607	0.000031	0.001263	0.000027	0.059873	353	−6.3	1.1	1.3	1.2
	FAM-177_4a	353	0.282667	0.000035	0.002556	0.000214	0.121723	353	−4.2	1.2	3.1	1.0
	FAM-177_3a	353	0.282651	0.000038	0.002223	0.000168	0.105691	353	−4.7	1.3	2.6	1.1
	FAM-177_2a	353	0.282632	0.000052	0.001272	0.000140	0.057944	353	−5.4	1.9	2.2	1.1
	FAM-177_1b	353	0.282628	0.000031	0.001679	0.000085	0.079175	353	−5.6	1.1	1.9	1.1
	FAM-177_1a	353	0.282716	0.000034	0.002703	0.000258	0.131327	353	−2.42	1.21	4.8	0.9
Average											2.6	1.1
ZAP-33	12/11											
	ZAP-33_12a	340	0.282409	0.000024	0.000482	0.000017	0.022801	340	−13.3	0.9	−5.9	1.6
	ZAP-33_11a	340	0.282409	0.000031	0.000685	0.000014	0.031634	340	−13.3	1.1	−5.9	1.6
	ZAP-33_10a	340	0.282424	0.000023	0.000577	0.000005	0.026810	340	−12.8	0.8	−5.3	1.6
	ZAP-33_9a	340	0.282379	0.000023	0.000926	0.000024	0.044627	340	−14.4	0.8	−7.0	1.7
	ZAP-33_8a	340	0.282407	0.000044	0.000616	0.000009	0.031501	340	−13.4	1.6	−5.9	1.6
	ZAP-33_7b	340	0.282396	0.000035	0.000576	0.000022	0.027877	340	−13.8	1.2	−6.3	1.7
	ZAP-33_5a	340	0.282438	0.000024	0.000453	0.000002	0.020572	340	−12.3	0.9	−4.8	1.6
	ZAP-33_3b	340	0.282447	0.000032	0.000851	0.000009	0.036220	340	−12.0	1.1	−4.6	1.5
	ZAP-33_3a	340	0.282431	0.000025	0.001165	0.000026	0.048962	340	−12.5	0.9	−5.2	1.6
	ZAP-33_2a	340	0.282394	0.000028	0.000615	0.000017	0.028751	340	−13.8	1.0	−6.4	1.7
	ZAP-33_1a	340	0.282401	0.000040	0.001311	0.000099	0.039749	340	−13.6	1.4	−6.3	1.6
Average											−5.8	1.6
VEL-6017[b]	10/10											
	VEL-6017_4a	340	0.282444	0.000057	0.001671	0.000140	0.062118	340	−12.1	2.0	−4.9	1.5
	VEL-6017_1a	340	0.282410	0.000080	0.001217	0.000077	0.050555	340	−13.3	2.8	−6.0	1.6
Average											−5.4	1.6
	VEL-6017_2a	340	0.282543	0.000057	0.000840	0.000073	0.033059	340	−8.5	2.0	−1.2	1.3
	VEL-6017_1b	340	0.282518	0.000071	0.000879	0.000206	0.040033	340	−9.4	2.5	−2.1	1.4
	VEL-6017_5b	340	0.282619	0.000073	0.000554	0.000007	0.028718	340	−5.9	2.9	1.6	1.2
	VEL-6017_3a	340	0.282574	0.000043	0.000367	0.000006	0.017919	340	−7.5	1.5	0.0	1.3
	VEL-6017_2b	340	0.282591	0.000049	0.000739	0.000033	0.037920	340	−6.9	1.7	0.6	1.2
Average											−0.2	1.3

[a] Total number of analyses/number chosen for εHf calculation.
[b] VEL-6017 defines two Hf compositions populations.

melt from which the zircons precipitated, from early to late crystallization stage. Considering the scale of our work, where the objective is to evaluate the predominant Hf isotopic compositions of the magma sources, we have calculated what we consider to be the most representative values for each sample. We have eliminated 'extreme' values (compare Table 2 and Supplementary Table 2) that diverge by more than ~3 ε$_{Hft}$ units (i.e., the total uncertainty estimated for individual analyses, see Section 3). Exceptions were made for FAM-7086 and VEL-6017 (see explanation below). In some cases no such filtering was necessary, e.g., when ε$_{Hft}$ values diverge by less than ~3 ε$_{Hft}$ units (Table 2, Supplementary Table 2). However, extreme values observed in some samples (Supplementary Table 2)

are taken into account in this study because they could represent variability in the main magma source (e.g., juvenile material contribution, deep metasediments, pre-existing crystalline basement) or contaminants (e.g., upper crustal wall-rocks).

5.2. Early–Middle Ordovician magmatism

The Early–Middle Ordovician magmatism is by far the most voluminous of the Sierras Pampeanas (Fig. 1) and is thus highly significant for crustal evolution in this region. These granitic rocks are calc-alkaline (composition in Supplementary Table 3) and represent an active continental margin. For these samples ε$_{Hft}$ and ε$_{Ndt}$ values

Table 3

Whole-rock Nd isotopes for Early–Middle Ordovician metaluminous plutonic rocks.

Sample	Lithology	Ages	Sm (ppm)	Nd (ppm)	$^{147}Sm/^{144}Nd$	$(^{143}Nd/^{144}Nd)_{today}$	$(^{143}Nd/^{144}Nd)t$	$\varepsilon Nd(t)$	T_{DM}† (Ga)
VCA-7037	Granodiorite	473	1.60	6.20	0.1592	0.512226	0.511733	−5.8	1.7
VCA-7038	Granodiorite	473	3.70	20.2	0.1098	0.512113	0.511773	−5.0	1.6
VCA-7040	Granodiorite	473	4.20	22.3	0.1144	0.512112	0.511758	−5.3	1.6
VCA-7039	Granodiorite	473	4.90	22.3	0.1323	0.512191	0.511781	−4.8	1.6
FAM-7086	Tonalite	473	14.2	59.4	0.1445	0.512172	0.511724	−5.9	1.7
FAM-7083	Monzogranite	473	7.70	36.6	0.1264	0.512270	0.511878	−2.9	1.4
RLC-243	Granodiorite	473	5.50	28.3	0.1172	0.512122	0.511759	−5.3	1.6
GUA-253	Tonalite	473	5.00	20.9	0.1455	0.512214	0.511763	−5.2	1.6
GUA-252	Aplite	473	1.80	5.40	0.1983	0.512370	0.511756	−5.3	1.6
MIS-259	Tonalite	473	8.80	40.0	0.1336	0.512200	0.511786	−4.7	1.6
PUL-244	Granodiorite	473	7.30	36.5	0.1213	0.512183	0.511807	−4.3	1.5
ELE-206	Monzogranite	473	6.10	26.0	0.1424	0.512173	0.511732	−5.8	1.7
NAC-257	Monzogranite	473	3.80	18.4	0.1264	0.512159	0.511767	−5.1	1.6
OLT-279	Monzogranite	473	4.90	19.1	0.1560	0.512221	0.511738	−5.7	1.6
OLT-282	Monzogranite	473	5.20	24.2	0.1292	0.512142	0.511742	−5.6	1.6
PAS-272	Granodiorite	473	5.50	27.5	0.1198	0.512119	0.511748	−5.5	1.6
SVF-577	Hbl-rich Gabbro	473	10.1	38.7	0.1582	0.512242	0.511752	−5.4	1.6
ANC-11022	Monzogranite	473	3.90	16.8	0.1412	0.512212	0.511779	−3.3	1.5
ANC-11030a	Tonalite	473	6.00	30.2	0.1198	0.512233	0.511863	−5.0	1.6
Average		473					0.511770	−5.1	1.7

Age average (473 Ma) was obtained from range of values (484–463 Ma) reported by Dahlquist et al. (2008). Average Nd isotopic composition excludes a few extreme values below −7.0 obtained from S-type granites. $(^{143}Nd/^{144}Nd)t$ CHUR = 0.512029, with t = 473 Ma.

Notes: 1. Early–Middle Ordovician data from Pankhurst et al. (1998, 2000) and Dahlquist et al. (2008, 2010). ANC-11030a from Dahlquist et al. (2012), Early Carboniferous data from Dahlquist et al. (2010), and Middle–Late Devonian data from this work, excepting ACH-5, ACH-15, ACH-23, and ACH-25 (Rapela et al., 2008b). 2. The decay constants used in the calculations are the values $\lambda^{147}Sm = 6.54 \times 10^{-12}$ year^{-1} recommended by the IUGS Subcommision for Geochronology (Steiger and Jäger, 1977). Epsilon-Nd (εNd) values calculated using the following CHUR parameters (Jacobsen and Wasserburg, 1980; Goldstein et al., 1984): $(^{143}Nd/^{144}Nd)_{today} = 0.512638$; $(^{143}Sm/^{144}Nd)_{today} = 0.1967$. t = time used for the calculation of the isotopic initial ratios.
† T_{DM} = calculated according to DePaolo et al. (1991).
§ VCA-6017 = SPB-9.
# CHI-7 produces an irreal T_{DM} value of −1.4 Ga.
VMA-1018 is a highly altered porphyritic monzogranite and the chemical analysis was not possible.

Whole-rock Nd isotopes for Late–Middle Devonian granitic rocks

Sample	Lithology	Age	Sm (ppm)	Nd (ppm)	$^{147}Sm/^{144}Nd$	$(^{143}Nd/^{144}Nd)_{today}$	$(^{143}Nd/^{144}Nd)t$	$\varepsilon Nd(t)$	T_{DM}† (Ga)
DAL-1	Felsic Granodiorite	369	11.5	57.7	0.1203	0.512200	0.511910	−5.0	1.5
ACH-140	Monzogranite	369	5.50	26.8	0.1248	0.512216	0.511915	−4.9	1.5
NPE-6	Monzogranite	369	8.80	43.3	0.1223	0.512152	0.511858	−6.0	1.6
NPE-14	Monzogranite	369	10.2	55.5	0.1112	0.512112	0.511843	−6.3	1.6
NPE-10	Bt-Ap bodies	369	159	709.	0.1358	0.512202	0.511875	−5.7	1.6
NPE-5	Bt-rich granite	369	17.6	87.6	0.1214	0.512148	0.511855	−6.0	1.6
ACH-154	Felsic Granodiorite	369	13.6	97.9	0.0841	0.512033	0.511830	−6.5	1.6
ACH-155	Monzogranite	369	8.90	50.2	0.1066	0.512104	0.511849	−6.2	1.6
ACH-5	Monzogranite	369	3.70	19.7	0.1128	0.512233	0.511961	−4.0	1.4
ACH-25	Monzogranite	369	6.20	32.5	0.1159	0.512239	0.511960	−4.0	1.4
ACH-23	Tonalite	369	6.40	39.0	0.1000	0.512341	0.512100	−1.2	1.2
ACH-15	Tonalite	369	7.10	35.9	0.1191	0.512354	0.512067	−1.9	1.3
Average		369					0.511919	−4.8	1.5

Age average (369 Ma) was obtained from ages reported in Table 1. Average excluding the tonalites, ACH-23 and 15 (see discussion in the text).

Whole-rock Nd isotopes for Early Carboniferous granitic rocks

Sample	Lithology	Age	Sm (ppm)	Nd (ppm)	$^{147}Sm/^{144}Nd$	$(^{143}Nd/^{144}Nd)_{today}$	$(^{143}Nd/^{144}Nd)t$	$\varepsilon Nd(t)$	T_{DM}† (Ga)
FIA-3	Monzogranite	341	12.1	67.1	0.1090	0.512351	0.512108	−1.8	1.3
FIA-8	Monzogranite	341	11.9	64.0	0.1124	0.512320	0.512069	−2.5	1.3
FIA-17	Monzogranite	341	12.1	51.5	0.1420	0.512434	0.512117	−1.6	1.2
FIA-18	Monzogranite	341	12.5	52.0	0.1453	0.512458	0.512134	−1.3	1.2
FIA-22	Monzogranite	341	11.2	61.7	0.1097	0.512406	0.512161	−0.7	1.2
HUA-4	Monzogranite	341	4.60	20.1	0.1383	0.512338	0.512029	−3.3	1.4
HUA-6	Monzogranite	341	10.2	46.5	0.1326	0.512365	0.512069	−2.5	1.3
HUA-7	Monzogranite	341	9.80	43.6	0.1359	0.512335	0.512032	−3.3	1.4
HUA-12	Monzogranite	341	10.5	49.1	0.1293	0.512352	0.512063	−2.6	1.3
HUA-13	Monzogranite	341	9.20	44.8	0.1241	0.512318	0.512041	−3.1	1.4
SBP-6	Monzogranite	341	17.0	82.1	0.1252	0.512234	0.511955	−4.8	1.5
SBP-9	Monzogranite	341	9.60	47.5	0.1222	0.512395	0.512122	−1.5	1.2
SBP-10	Monzogranite	341	16.8	73.9	0.1374	0.512537	0.512230	0.6	1.1
SBP-15	Monzogranite	341	11.1	59.5	0.1128	0.512365	0.512113	−1.7	1.2
ZAP-26	Monzogranite	341	17.1	92.3	0.1120	0.512258	0.512008	−3.7	1.4
ZAP-27	Monzogranite	341	18.6	69.6	0.1616	0.512430	0.512069	−2.5	1.3
ZAP-29	Monzogranite	341	15.1	64.5	0.1415	0.512366	0.512050	−2.9	1.3

Table 3 (continued)

Sample	Lithology	Ages	Sm (ppm)	Nd (ppm)	$^{147}Sm/^{144}Nd$	$(^{143}Nd/^{144}Nd)_{today}$	$(^{143}Nd/^{144}Nd)t$	$\varepsilon Nd(t)$	T_{DM} (Ga)
ZAP-33	Monzogranite	341	9.70	46.3	0.1266	0.512306	0.512023	−3.4	1.4
CHI-7	Monzogranite	341	6.62	14.8	0.2700	0.512663	0.512060	−2.7	1.3
FAM-177	Monzogranite	341	9.47	53.5	0.1070	0.512403	0.512164	−0.7	1.2
Average		341					0.512081	−2.3	1.3

Age average (341 Ma) was obtained from ages reported in Table 1.

range from −3.3 to −14.2 and −3.3 to −6.3, respectively, with average T_{DM} Hf and T_{DM} Nd values ranging from 1.5 to 2.2 Ga and 1.4 to 1.7 Ga, respectively (Tables 1–3 and Fig. 2). Sample FAM-7086, in particular, has a very low zircon ε_{Hft} average of −14.2 and a whole-rock ε_{Ndt} value of −5.9 (Table 3). The most mafic rock (SVF-577 with $SiO_2 = 42.6\%$) has negative Hf and Nd isotope compositions with an ε_{Hft} average of −5.7 and a whole-rock ε_{Ndt} value of −5.4 (Tables 2 and 3). The few extreme values observed in the samples ANC-11030a, FAM-7086, and SVF-577 are reported in Supplementary Table 2 and discussed in Section 6.

5.3. Middle–Late Devonian magmatism

During the Middle–Late Devonian, magmatism was developed in a foreland position away from the orogenic front in the west (Fig. 1). F-U-REE rich A-type granites formed at this time (composition in Supplementary Table 3). The analyzed plutonic rocks from Achala batholith have ε_{Hft} and ε_{Ndt} values ranging from −3.6 to −5.8 and -4.0 to −6.5, respectively (Tables 1–3 and Fig. 2). Average T_{DM} Hf and T_{DM} Nd values range from 1.5 to 1.6 and 1.4 to 1.6, respectively (Tables 2 and 3). More negative ε_{Hft} values (ranging from −10.7 to −17.6) were observed in one sample only (ACH-140, Supplementary Table 2).

5.4. Early Carboniferous magmatism

The Early Carboniferous A-type granites (composition in Supplementary Table 3) have ε_{Hft} and ε_{Ndt} values ranging from −6.7 to +2.6 and −0.5 to −3.6, respectively (Tables 1–3 and Fig. 2). Extreme negative ε_{Hft} values are observed in samples FIA-17, HUA-12, and ZAP-33 (Supplementary Table 2). A distinctive zircon ε_{Hft} composition is revealed by FAM-177, with dominantly positive ε_{Hft} values (Table 2). VEL-6017 zircons show two contrasting isotopic compositions, defining positive and negative ε_{Hft} values, respectively (Table 2).

6. Implications for crustal growth on the proto-Andean margin of Gondwana

6.1. Early–Middle Ordovician magmatism

Zircon Hf and whole-rock Nd isotopic signatures in the Early–Middle Ordovician calc-alkaline granitoids indicate magmas dominated by pre-existing continental crust (Fig. 2) as suggested by Pankhurst et al. (2000), Rapela et al. (2008a), and Dahlquist et al. (2008). As argued by Rapela et al. (2008a), the classical Andean model for magma generation invoking a strong mantle contribution (e.g., Pitcher, 1979; Wilson, 1989; Parada et al., 1999; Hervé et al., 2007; and references therein) does not seem to apply to these Ordovician calc-alkaline granites.

The few extreme zircon ε_{Hft} values observed in some samples of Ordovician age (ANC-11030a, FAM-7086, and SVF-577, Supplementary Table 2) do not significantly change the conclusion that rather consistently old continental sources were involved in Famatinian magmatism, although they suggest that some samples were contaminated by different older continental materials with distinctive isotopic signature (e.g., deep crystalline basement or upper crustal wall-rocks such as metasediments).

Previous analyses of mafic rocks from Sierra de Valle Fértil, ranging from olivine-bearing gabbronorites to pyroxene–hornblende gabbros, produced negative ε_{Ndt} values ranging from −2.4 to −5.6 (7 analyses, Pankhurst et al., 2000) and −2.6 to −5.1 (4 analyses, Otamendi et al., 2012). Only two slightly positive epsilon values (+0.25 and +0.9) have been reported for two pyroxene–hornblende gabbros (Otamendi et al., 2009, 2012). Intermediate and felsic granitoids in Sierra de Valle Fértil mostly have ε_{Ndt} values ranging from −4.4 to −6.0 (18 samples), with two negative values of −3.0 and -3.4, and three highly negative values of −7.2, −7.3 and −8.7 (Otamendi et al., 2012). Therefore, the data strongly suggest that these gabbros were mainly derived from lithospheric mantle. As suggested by Pankhurst et al. (2000), depleted mantle model ages (T_{DM}) indicate derivation from dominantly Mesoproterozoic sources. The slightly positive epsilon values from the two gabbros could represent a more juvenile magma ascending through local conduits during the development of the Famatinian arc, but without significant participation in the generation of the large parental Famatinian magmatism. However, there is no conclusive evidence on this issue.

The dominantly negative zircon ε_{Hft} from the hornblende-bearing gabbro SVF-577 reported in this work also indicates an old lithospheric source. Since early-crystallizing zircon would retain the original isotope signature of the parental melt (e.g., Kemp et al., 2007), the absence of juvenile material in all analyzed zircons strongly supports magma derivation from the continental lithosphere (Fig. 3a).

Based on U–Pb SHRIMP detrital zircon dating and P–T conditions of metamorphism of high-grade migmatitic gneisses from the Loma de Las Chacras (Fig. 1), Casquet et al. (2012) conclude that the sedimentary protoliths were deposited essentially coevally with Famatinian magmatism at ca. 468 ± 3 Ma and that they were buried and metamorphosed at high pressure (ca. 1.2 GPa) and high temperature (ca. 780 °C) soon after sedimentation. These metamorphic conditions contrast strongly with the typical low-P and high-T metamorphism reported in the Famatinian belt of Sierras Pampeanas (e.g., Pankhurst et al., 1998; Dahlquist, 2001; Dahlquist et al., 2005, 2007; Otamendi et al., 2008). Casquet et al. (2012) indicate that the structural position of the Loma de Las Chacras relative to the Valle Fértil igneous–metamorphic belt suggests that in the former case burial took place outboard of the magmatic arc and that these metasediments underplated the arc. These authors suggest that the Loma de Las Chacras metasedimentary rocks may have been laid down in a forearc basin far from the leading edge of the overriding plate.

In Loma de Las Chacras, Casquet et al. (2012) describe amphibolites that represent swarms of former dykes transported into parallelism with the foliation of the host migmatite. The Loma de Las Chacras amphibolites have a depleted-source Nd isotopic signature: three samples have positive ε_{Ndt} ranging from +1.8 to +4.8, with one at −0.1. Casquet et al. (2012) emphasize that the juvenile signature of the amphibolites is very unusual for basic rocks associated with Famatinian magmatism, which generally show more evolved Nd and Sr isotopic characteristic (e.g., Pankhurst et al., 1998, 2000; Dahlquist et al., 2008;

Otamendi et al., 2012). Hence, they conclude that the juvenile material was injected into buried sediments outboard of the magmatic arc.

6.2. Middle–Late Devonian magmatism

Hf and Nd data from the Achala granites suggest that these A-type granitic magmas were also largely derived from the recycling of old crustal rocks (Fig. 2). Consistent with this conclusion are the zircon
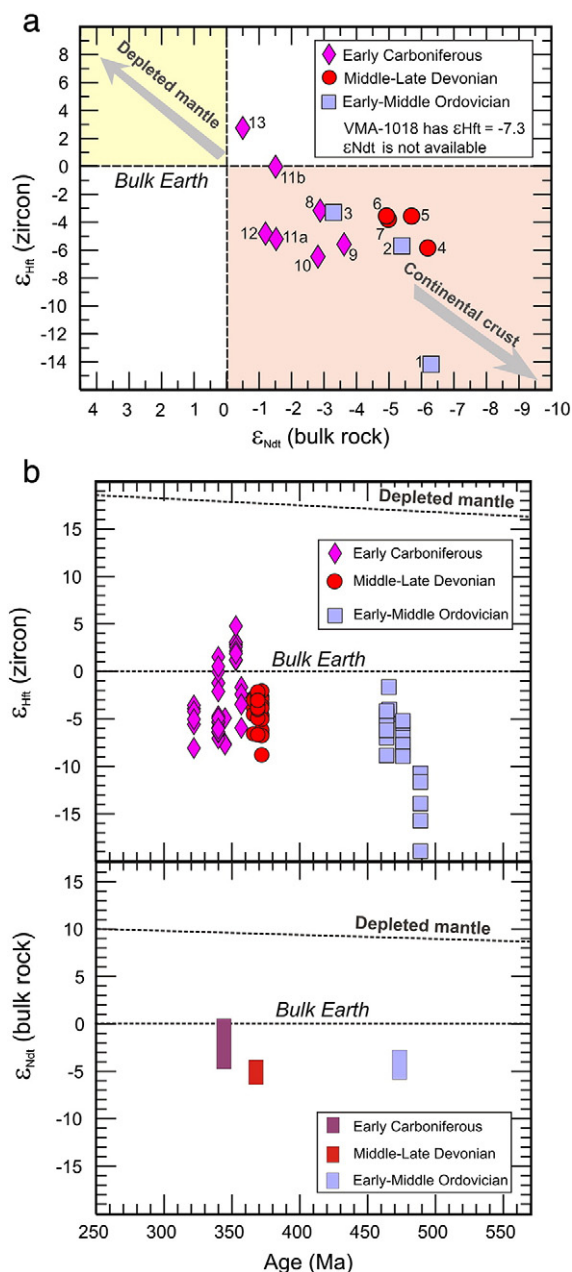

Fig. 2. (a) Average ε_{Hft} isotope composition of melt-precipitated zircons from samples of each suite as a function of whole-rock ε_{Ndt} isotope composition at the time of crystallization of the granitic rocks of Sierras Pampeanas. Average ε_{Hft} values from Table 2 (with crystallization ages in Ma): 1 = FAM-7086 (489), 2 = SVF-577 (464), 3 = ANC-11030a (466), 4 = NPE-14 (369), 5 = NPE-10 (369), 6 = DAL-1 (372), 7 = ACH-140 (366), 8 = HUA-12 (357), 9 = ZAP-33 (340), 10 = CHI-17 (345), 11a = VEL-6017 (340), 11b = VEL-6017 (340), 12 = FIA-17 (322), and 13 = FAM-177 (353). (b) Above: ε_{Hft} values for magmatic zircons plotted as a function of crystallization age. VEL-6017 defines two Hf composition populations (see text and Table 2). Below: ε_{Ndt} values from whole-chemistry rocks reported in Table 3. Anomalous values of small tonalites from Achala batholith are not plotted. The depleted mantle evolution curves for Hf and Nd are from Kemp et al. (2006) and Goldstein et al. (1984), respectively.

age patterns of porphyritic granites reported by Rapela et al. (2008b), which show inherited components commonly found in the Cambrian metasedimentary country rocks of the batholith and therefore are likely a source component for these granites. However, Rapela et al. (2008b) have suggested the Achalian granites cannot be entirely derived from a Pampean basement source, since the Nd isotopic composition of the basement is well bracketed within an even more 'crustal' isotopic range ($\varepsilon_{Nd520} = -4.5$ to -7.5; Rapela et al., 2008b). Rapela et al. (2008b, data listed in Table 3) reported similar ε_{Ndt} (-4.0) for monzogranites from the same batholith. They found rather more radiogenic Nd in small tonalite and leucogranites bodies ($\varepsilon_{Ndt} = -1.2$ to -1.9, mean $= -1.6$, and $\varepsilon_{Ndt} = -1.1$ to -1.4, respectively). However, these minor intrusions could represent a more juvenile magma ascending through hypothetical local conduits, although further studies are required to test this hypothesis.

As noted by Nelson (1992), high abundances of P_2O_5 (up to 3.3 wt.%) and of volatiles such as F (up to 1%) could be readily explained by the involvement of sediment in the source. Achala granites have biotite with very high F content (mean $= 2.1$%); they bear unusual enclaves characterized by 89–93% biotite with high FeO/MgO ratios (mean 3.1) and 7–11% apatite with high F contents (mean 3.5%); and they have abundant zircon and monazite together with scarce oxides as accessory minerals (data from Dorais et al., 1997). The modal mineralogy produces unusual bulk-rock compositions, including enhanced $P_2O_5 = 5.4$ wt.%, F~6–7 wt.%, and very high U $= 181$ ppm, Zr (2581 ppm) and $\Sigma REEs = 4500$ ppm contents (see NPE-10 sample in Supplementary Table 3). The ε_{Hft} and ε_{Ndt} data reported here strongly suggest a dominant older crustal component, and a scenario similar to that shown in Fig. 3b is assumed for the generation of A-type magmas during the Middle–Late Devonian. Significantly more negative values of ε_{Hft} were observed in sample ACH-140 (Supplementary Table 2), suggesting contamination by much older metasediments at depth. We have therefore incorporated a petrogenetic scenario involving sediment contamination (Fig. 3b) following the geodynamic model discussed by Alasino et al. (2012) for the Late Paleozoic.

6.3. Early Carboniferous magmatism

Grosse et al. (2009) and Fogliata et al. (2012) reported the presence of zircons with Carboniferous crystallization ages in granites containing inherited zircon with Ordovician ages, and consequently invoked significant participation of Ordovician meta-granitoids in the source of the Early Carboniferous A-type granites. However, the Carboniferous magmas could not have been entirely derived by remelting of the Ordovician granites because their ε_{Ndt} values are less negative ($+0.6$ to -4.8 at 323 to 354 Ma) than those of the Famatinian granitoids of 320–360 Ma (-4.8 to -8.5, Dahlquist et al., 2010; see also Grosse et al., 2009). Thus, the additional participation of an asthenospheric component is required to satisfy the ε_{Ndt} and ε_{Hft} values calculated for the Early Carboniferous granitoids. Recently, Alasino et al. (2012) concluded that the Carboniferous granitic rocks overall show west-to-east mineralogical and isotopic regional zonation indicating that magma genesis involved a greater contribution of juvenile material of mantle character towards the west. The felsic-to-intermediate component in a mixture is likely to dominate the Sm–Nd composition of the resultant magma due to its higher Sm and Nd contents. As reported by Kemp et al. (2007), when supracrustal material is reworked by juvenile magmas the Nd isotope ratios of the resulting bulk magma can camouflage the juvenile component. Conversely, the zircon can crystallize sufficiently early to retain vestiges of the original isotope signature. Kemp et al. (2007) concluded that mafic magmas in the Lachlan Fold Belt (SE Australia) were subsequently modified by strong crustal contamination, as is evident in the spread of zircon ε_{Hft} and δO^{18} values in the Why Worry basalt (ε_{Hft} values ranging from ca. -8 to $+6$), but

zircon crystallized sufficiently early and retained vestiges of the original (juvenile) isotope signature. Thus, the zircon Hf data can be considered more robust in constraining the source of the Early Carboniferous A-type magmas. The ε_{Hft} values reported here are consistent with the conclusions of Alasino et al. (2012) implying

continental growth by addition of juvenile material in a foreland region, in particular for the Cerro La Gloria pluton with $\varepsilon_{Hft} = +2.6$ (Fig. 1 and Table 2). Thus, a petrogenetic model invoking interaction between crust of hypothetical Ordovician and Mesoproterozoic ages and juvenile magmas could be applied to the generation of Eastern
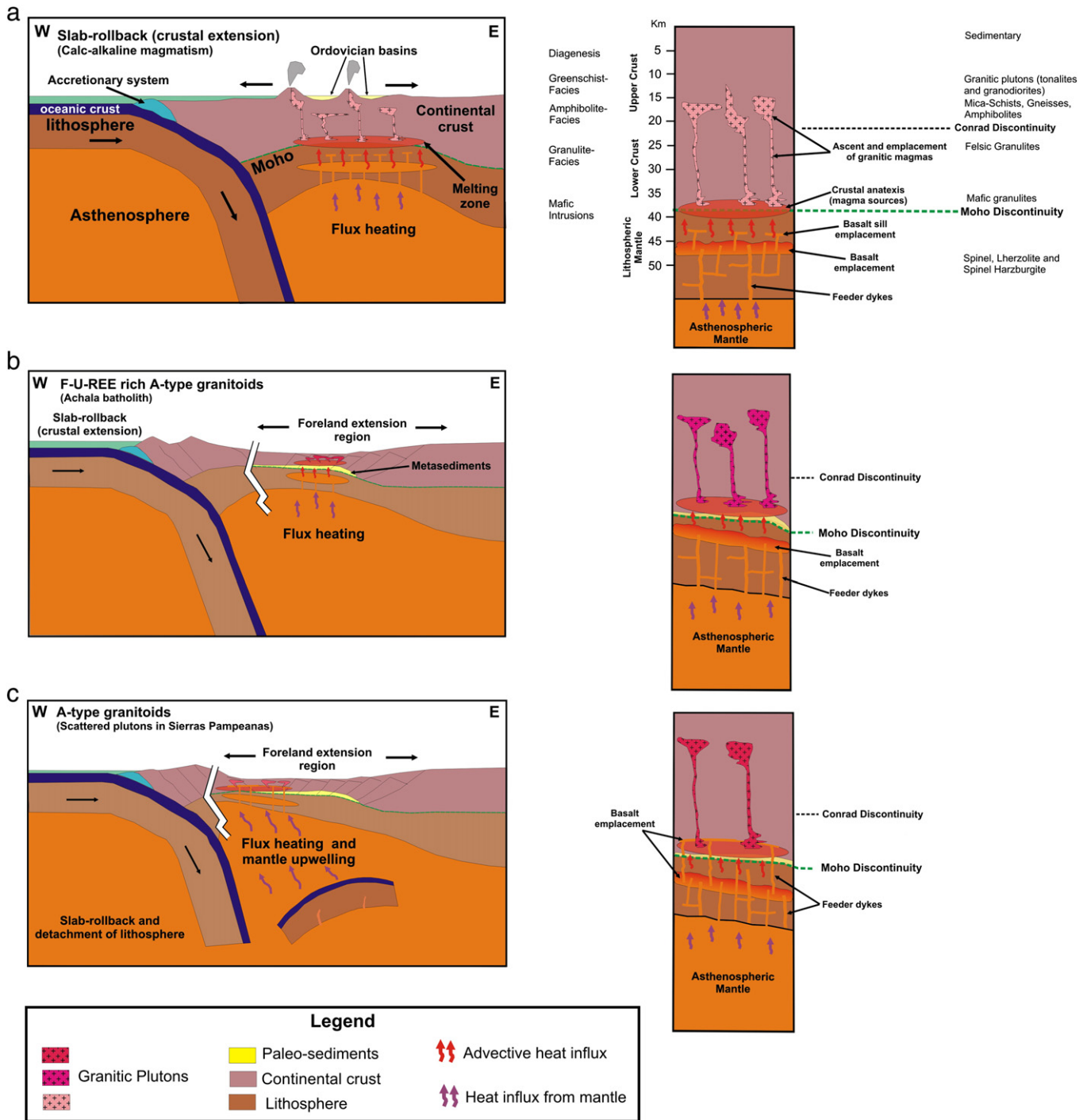
Fig. 3. Possible schematic geodynamic scenario for magma generation in the proto-Andean margin of Gondwana between 32° and 26°S during the Paleozoic (see Fig. 1). Cartoon of the standard profile of the continental crust, modified from Wedepohl (1995). Generalized location for each magmatic event in Fig. 1: (a) Early–Middle Ordovician magma generation in a roll-back subduction setting, (b) Middle–Late Devonian, and (c) Early Carboniferous magma generation in a dominant extensional regime with subsequent lithosphere thinning. Detachment of the lithosphere is included in this setting. Final emplacement of Achala granites is in a dominantly compressional regime (see discussion in the text). Ascent of magmas during the Early Carboniferous (and probably during the Middle–Late Devonian) was facilitated by shear zones (see discussion in the text). The probable source for each setting is: (a) Early–Middle Ordovician: Mesoproterozoic continental crust (T_{DM} Hf = 1.5–2.2 Ga and T_{DM} Nd = 1.4–1.7 Ga), supporting an absent asthenospheric mantle contribution; (b) Middle–Late Devonian and (c) Early Carboniferous: mainly the Sierra de Córdoba basement and Ordovician granites, respectively. (b) and (c) support a Mesoproterozoic continental crust source (see T_{DM} Hf and T_{DM} Nd in Tables 2 and 3) with variable mantle contribution during the Early Carboniferous (see discussion in the text). The presence of paleo-sediment in the source for settings (b) and (c) was included in agreement with the geotectonic scenario discussed by Alasino et al. (2012). Complete references for the three figures are in subpanel a.

Sierras Pampeanas magmas during the Early Carboniferous (Fig. 3c). The presence of sediment in the source of the Early Carboniferous granites was invoked by Alasino et al. (2012) to explain anomalously high concentrations of some trace elements. These authors indicate that the juvenile contribution to the Carboniferous magmatism could be explained by detachment of the lithosphere. We have therefore incorporated a petrogenetic scenario involving sediment contamination and detachment of the lithosphere in our geodynamic model shown in Fig. 3c.

6.4. Previous U–Pb and Lu–Hf isotope studies of the proto-Andean margin of Gondwana

In recent years several studies have presented LA-ICP-MS U–Pb ages and Hf-isotope data for detrital zircons from Paleozoic metasediments of the accretionary systems on the western margin of South America (Chile, Peru, and Bolivia), in order to trace the evolution of continental crust on the proto-Andean margin of Gondwana (e.g., Willner et al., 2008; Bahlburg et al., 2009; Reimann et al., 2010 and references therein). In particular, the crustal evolution of the region studied here was assessed by Willner et al. (2008) and Bahlburg et al. (2009) using data for detrital zircon in Late Paleozoic coastal accretionary systems in central Chile and the Guarguaráz complex in W Argentina (29°–36° L.S.). Several of our conclusions are consistent with theirs, confirming earlier Nd isotope evidence (e.g., Pankhurst et al., 2000; Dahlquist et al., 2008 and references therein) that the Famatinian granites originated by recycling mainly Mesoproterozoic crust, whereas zircons from Carboniferous igneous sources reflect either crustal contamination of juvenile parent magmas or, more likely, recycling of more juvenile crustal material (Willner et al., 2008; Alasino et al., 2012).

Miskovic and Schaltegger (2009) carried out extensive geochemical characterization and an in situ U–Pb and Lu–Hf isotopic study of igneous zircon from granitoid batholiths that form the backbone of the Eastern Cordillera of Peru. Studied granitoids associated with phases of regional compressive tectonism correspond to mean initial ε_{Hft} values of -6.7, -2.4, -1.6 for the Ordovician (Famatinian), Carboniferous–Permian and Late Triassic respectively, suggesting a minimum crustal contribution of between 40% and 74% by mass. Remarkably, positive ε_{Hft} values are absent in Famatinian granitoids and are reported only for Carboniferous–Permian magmatism.

In Argentina, previous U–Pb and Hf determinations on magmatic zircons from small outcrops of Famatinian meta-igneous rocks in La Pampa province (U–Pb zircon SHRIMP ages ranging from ca. 476 to 466 Ma) reveal similar results to those presented here, with negative ε_{Hft} values from -3.6 to -5.0 and average Lu–Hf two stages model ages of ca. 1.7 Ga (Chernicoff et al., 2010).

7. Conclusions

The data presented here confirm previous work indicating that the Early–Middle Ordovician magmas of the Famatinian arc were largely derived by melting of pre-existing old crustal rocks, without evident participation of the asthenospheric mantle. As noted above, the Early–Middle Ordovician magmatism is by far the most voluminous magmatism in the Sierras Pampeanas and represents the main magmatic event in the crustal development of this region of the proto-Andean margin of Gondwana. The Middle–Late Devonian magmas resulted from reworking of supracrustal material in a foreland region, whereas the Early Carboniferous magmas resulted in part from reworking of supracrustal material in a largely cratonized region, but with variable contribution of juvenile magmas.

Supplementary data to this article can be found online at http://dx.doi.org/10.1016/j.gr.2012.08.013.

References

Aceñolaza, F.G., Miller, H., Toselli, A.J., 1996. Geología del Sistema de Famatina. In: Aceñolaza, F.G., Miller, H., Toselli, A.J. (Eds.), Geología del Sistema de Famatina: Münchner Geologische Hefte, Reihe A, 19(6). 412 pp.

Alasino, P.H., Dahlquist, J.A., Pankhurst, R.J., Galindo, C., Casquet, C., Rapela, C.W., Larrovere, M., Fanning, C.M., 2012. Early Carboniferous sub- to mid-alkaline magmatism in the Eastern Sierras Pampeanas. NW Argentina: a record of crustal growth by the incorporation of mantle-derived material in an extensional setting. Gondwana Research 22, 992–1008. http://dx.doi.org/10.1016/j.gr.2011.12.011.

Bahlburg, H., Vervoort, J.D., DuFrane, S.A., Bock, B., Augustsson, C., 2009. Timing of accretion and crustal recycling at accretionary orogens: insights learned from the western margin of South America. Earth-Science Reviews 97, 227–253.

Baldo, 1992. Estudio petrológico y geoquímico de las rocas ígneas y metamórficas entre Pampa de Olaen y Characato. Extremo norte de la Sierra Grande de Córdoba. República Argentina. Tesis Doctoral, Universidad Nacional de Córdoba, (unpublished). pp. 305.

Bouvier, A., Vervoort, J.D., Hatchett, J.P., 2008. The Lu–Hf and Sm–Nd isotopic composition of CHUR: constraints from unequilibrated chondrites and implications for the bulk composition of terrestrial planets. Earth and Planetary Science Letters 273, 48–57.

Casquet, C., Rapela, C.W., Pankhurst, R.J., Baldo, E.G., Galindo, C., Fanning, C.M., Dahlquist, J.A., 2012. Fast sediment underplating and essentially coeval juvenile magmatism in the Ordovician margin of Gondwana, Western Sierras Pampeanas, Argentina. Gondwana Research 22, 664–673.

Cawood, P.A., 2005. Terra Australis Orogen: Rodinia breakup and development of the Pacific and Iapetus margins of Gondwana during the Neoproterozoic and Paleozoic. Earth-Science Reviews 69, 249–279.

Cawood, P.A., Kröner, A., Collins, W.J., Kusky, T.M., Mooney, W.D., Windley, B.F., 2009. Accretionary orogens through Earth history. In: Cawood, P.A., Kröner, A. (Eds.), Geological Society, London, Special Publications, 318, pp. 1–36.

Chang, Z., Vervoort, J.D., McClelland, W.C., Knaack, C., 2006. U–Pb dating of zircon by LA-ICP-MS. Geochemistry, Geophysics, Geosystems 7 (Q05009), 1–14.

Chernicoff, C.J., Zappettini, E.O., Santos, J.O.S., Allchurch, S., McNaughton, N.J., 2010. The southern segment of the Famatinian magmatic arc, La Pampa Province, Argentina. Gondwana Research 17, 662–675.

Collins, W.J., 2002. Hot orogens, tectonic switching, and creation of continental crust. Geology 30, 535–538.

Dahlquist, J.A., 2001. Low-pressure emplacement of epidote-bearing metaluminous granitoids in the Sierra de Chepes (Famatinian orogen, Argentina) and relationships with the magmas sources. Revista Geológica de Chile 28, 147–161.

Dahlquist, J.A., 2002. Mafic microgranular enclaves: early segregation from metaluminous magma (Sierra de Chepes), Pampean Ranges, NW Argentina. Journal of South American Earth Sciences 15, 643–655.

Dahlquist, J.A., Galindo, C., 2004. Geoquímica isotópica de los granitoides de la sierra de Chepes: un modelo geotectónico y termal, implicancias para el orógeno famatiniano. Revista de la Asociación Geológica Argentina 59, 57–69.

Dahlquist, J.A., Rapela, C.W., Baldo, E.G., 2005. Cordierite-bearing S-Type granitoids in the Sierra de Chepes (Sierras Pampeanas): petrogenetic implications. Journal of South American Earth Sciences 20, 231–251.

Dahlquist, J.A., Pankhurst, R.J., Rapela, C.W., Casquet, C., Fanning, C.M., Alasino, P., Baez, F.M., 2006. The San Blas Pluton: an example of Carboniferous plutonism in the Sierras Pampeanas, Argentina. Journal of South American Earth Sciences 20, 341–350.

Dahlquist, J.A., Galindo, C., Pankhurst, R.J., Rapela, C.W., Alasino, P.H., Saavedra, J., Fanning, C.M., 2007. Magmatic evolution of the Peñón Rosado granite: petrogenesis of garnet-bearing granitoids. Lithos 95, 177–207.

Dahlquist, J.A., Pankhurst, R.J., Rapela, C.W., Galindo, C., Alasino, P., Fanning, C.M., Saavedra, J., Baldo, E., 2008. New SHRIMP U–Pb data from the Famatina Complex: constraining Early–Mid Ordovician Famatinian magmatism in the Sierras Pampeanas, Argentina. Geologica Acta 6, 319–333.

Dahlquist, J.A., Alasino, P.H., Eby, G.N., Galindo, C., Casquet, C., 2010. Fault controlled Carboniferous A-type magmatism in the proto-Andean foreland (Sierras Pampeanas, Argentina): geochemical constraints and petrogenesis. Lithos 115, 65–81.

Dahlquist, J.A., Rapela, C.W., Pankhurst, R.J., Fanning, C.M., Vervoort, J.D., Hart, G., Baldo, E.G., Murra, J.A., Alasino, P.H., Colombo, F., 2012. Age and magmatic evolution of the Famatinian granitic rocks of Sierra de Ancasti, Sierras Pampeanas, NW Argentina. Journal of South American Earth Sciences 34, 10–25.

DePaolo, D.J., Linn, A.M., Schubert, G., 1991. The continental crustal age distribution: methods of determining mantle separation ages from Sm–Nd isotopic data and application to the southwestern United States. Journal of Geophysical Research 96, 2071–2088.

Dickinson, W.R., Gehrels, G.E., 2003. U–Pb ages of detrital zircons from Permian and Jurassic eolian sandstones of the Colorado Plateau, USA: paleogeographic implications. Sedimentary Geology 163, 29–66.

Dorais, M., Lira, R., Chen, Y., Tingey, D., 1997. Origin of biotite–apatite-rich enclaves, Achala Batholith, Argentina. Contributions to Mineralogy and Petrology 130, 31–46.

Ducea, M.N., Otamendi, J.E., Bergantz, G., Stair, K.M., Valencia, V.A., Gehrels, G.E., 2010. Timing constraints on building an intermediate plutonic arc crustal section: U–Pb zircon geochronology of the Sierra Valle Fértil–La Huerta, Famatinian arc, Argentina. Tectonics 29 (TC4002), 21–22.

Fogliata, A.S., Báez, M.A., Hagemann, S.G., Santos, J.O., Sardi, F., 2012. Post-orogenic, Carboniferous granite-hosted Sn–W mineralization in the Sierras Pampeanas Orogen, Northwestern Argentina. Ore Geology Reviews 45, 16–32.

Gaschnig, R.M., Vervoort, J.D., Lewis, R.S., McClelland, W.C., 2010. Migrating magmatism in the northern US Cordillera: in situ U–Pb geochronology of the Idaho batholiths. Contributions to Mineralogy and Petrology 159, 863–883.

Goldstein, S.J., O'Nions, R.K., Hamilton, P.J., 1984. A Sm.Nd isotopic study of atmospheric dusts and particulates from major river systems. Earth and Planetary Science Letters 70, 221–236.

Goodge, J.W., Vervoort, J.D., 2006. Origin of Mesoproterozoic A-type granites in Laurentia: Hf isotope evidence. Earth and Planetary Science Letters 243, 711–731.

Grissom, G.C., Debari, S.M., Snee, L.W., 1998. Geology of the Sierras de Fiambalá, northwestern Argentina: implications for Early Palaeozoic Andean tectonics. In: Pankhurst, R.J., Rapela, C.W. (Eds.), The Proto-Andean Margin of Gondwana: Journal of the Geological Society, London, Special Publications, 142, pp. 297–323.

Grosse, P., Söllner, F., Baéz, M.A., Toselli, A.J., Rossi, J.N., de la Rosa, J.D., 2009. Lower Carboniferous post-orogenic granites in central-eastern Sierra de Velasco, Sierras Pampeanas, Argentina: U–Pb monazite geochronology and Sr–Nd isotopes. International Journal of Earth Sciences 98, 1001–1025.

Grosse, P., Bellos, L.I., de los Hoyos, C.R., Larrovere, M.A., Rossi, J.N., Toselli, A.J., 2011. Across-arc variation of the Famatinian magmatic arc (NW Argentina) exemplified by I-, S- and transitional I/S-type Early Ordovician granitoids of the Sierra de Velasco. Journal of South American Earth Sciences 32, 110–126.

Hawkesworth, C.J., Dhuime, B., Pietranik, A.B., Cawood, P.A., Kemp, A.I.S., Storey, C.D., 2010. The generation and evolution of the continental crust. Journal of the Geological Society of London 167, 229–248.

Hervé, F., Pankhurst, R.J., Fanning, C.M., Calderón, M., Yaxley, G.M., 2007. The South Patagonian batholith: 150 my of granite magmatism on a static plate margin. Lithos 97, 373–394.

Höckenreiner, M., Söllner, F., Miller, H., 2003. Dating the TIPA shear zone: an early Devonian terrane boundary between the Famatinian and Pampean systems (NW Argentina). Journal of South American Earth Sciences 16, 45–66.

Jacobsen, S.B., Wasserburg, G.J., 1980. Sm–Nd isotopic evolution of chondrites. Earth and Planetary Science Letters 50, 139–155.

Johnson, D.M., Hooper, P.R., Conrey, R.M., 1999. XRF analysis of rocks and minerals for major and trace elements on a single low dilution Litetraborate fused bead. Advances in X-ray Analysis 41, 843–867.

Kemp, A.I.S., Hawkesworth, C.J., Paterson, B.A., Kinny, P.D., 2006. Episodic growth of the Gondwana supercontinent from hafnium and oxygen isotopes in zircon. Nature 439, 580–583.

Kemp, A.I.S., Hawkesworth, C.J., Foster, G.L., Paterson, G.A., Woodhead, J.D., Hergt, J.M., Gray, C.M., Whitehouse, M.J., 2007. Magmatic and crustal differentiation history of granitic rocks from Hf–O isotopes in zircon. Science 315, 980–983.

Kosler, J., Sylvester, P.J., 2003. Present trends and the future of zircon in geochronology: laser ablation ICPMS. In: Hanchar, J.M., Hoskin, P.W.O. (Eds.), Zircon: Reviews in Mineralogy and Geochemistry, 53, pp. 243–276.

Llambías, E.J., Sato, A.M., Ortiz Suárez, A., Prozzi, C., 1998. The granitoids of the Sierra de San Luis. In: Pankhurst, R.J., Rapela, C.W. (Eds.), The Proto-Andean margin of Gondwana: Geological Society of London, Special Publications, 142, pp. 325–341.

López de Luchi, M.G., Rapalini, A.E., Siegesmund, S., Steenken, A., 2004. Application of magnetic fabrics to the emplacement and tectonic history of Devonian granitoids in central Argentina. In: Martín-Hernández, F., Lüneburg, F., Aubourg, C., y Jackson, M. (Eds.), Magnetic fabric: methods and applications: Geological Society, London, Special Publications, 238, pp. 447–474.

McBride, S.L., 1972. A Potassium–argon age investigation of igneous and metamorphic rocks from Catamarca and La Rioja provinces, Argentine. PhD. Thesis. Queen's University (unpublished). Ontario. Canada.

McBride, S.L., Caelles, J.C., Clark, A.H., Farrar, E., 1976. Paleozoic radiometric age provinces in the Andean basement, latitudes 25°–30°S. Earth and Planetary Science Letters 29, 373–383.

Miller, H., Söllner, F., 2005. The Famatina complex (NW-Argentina): back-docking of an island arc or terrane accretion? Early Palaeozoic geodynamics at the western Gondwana margin. In: Vaughan, A.P.M., Leat, P.T., Pankhurst, R.J. (Eds.), Terrane processes at the margins of Gondwana: Geological Society of London, Special Publication, 246, pp. 241–256.

Miskovic, A., Schaltegger, U., 2009. Crustal growth along a non-collisional cratonic margin: a Lu–Hf-isotopic survey of the Eastern Cordilleran granitoids of Peru. Earth and Planetary Science Letters 279, 303–315.

Nelson, D.R., 1992. Isotopic characteristic of potassic rocks. Evidence for the involvement of subducted sediment in magma genesis. Lithos 28, 403–420.

Otamendi, J.E., Tibaldi, A.M., Vujovich, G.I., Viñao, G.A., 2008. Metamorphic evolution of migmatites from the deep Famatinian arc crust exposed in Sierras Valle Fértil-La Huerta, San Juan, Argentina. Journal of South American Earth Sciences 25, 313–335.

Otamendi, J.E., Ducea, M.N., Tibaldi, A.M., Bergantz, G., de la Rosa, J.D., Vujovich, G.I., 2009. Generation of tonalitic and dioritic magmas by coupled partial melting of gabbroic and metasedimentary rocks within the deep crust of the Famatinian magmatic arc, Argentina. Journal of Petrology 50, 841–873.

Otamendi, J.E., Ducea, M.N., Bergantz, G.W., 2012. Geological, petrological and geochemical evidence for progressive construction of an arc crustal section, Sierra deValle Fertil, Famatinian Arc, Argentina. Journal of Petrology 53, 761–800.

Paces, J.B., Miller, J.D., 1993. Precise U–Pb ages of Duluth Complex and related mafic intrusions, north-eastern Minnesota: geochronological insights to physical, petrogenetic, paleomagnetic, and tectonomagmatic processes associated with the 1.1 Ga midcontinental rift system. Journal of Geophysical Research 98, 13997–14013.

Pankhurst, R.J., Rapela, C.W., 1998. The proto-Andean margin of Gondwana: an introduction. In: Pankhurst, R.J., Rapela, C.W. (Eds.), The proto-Andean margin of Gondwana: Geological Society, London, Special Publications, vol. 142, pp. 1–9.

Pankhurst, R.J., Rapela, C.W., Saavedra, J., Baldo, E.G., Dahlquist, J.A., Pascua, I., Fanning, C.M., 1998. The Famatinian arc in the central Sierras Pampeanas: an Early to Mid-Ordovician continental arc on the Gondwana margin. In: Pankhurst, R.J., Rapela, C.W. (Eds.), The Proto-Andean Margin of Gondwana: Geological Society of London, Special Publication, 142, pp. 343–367.

Pankhurst, R.J., Rapela, C.W., Fanning, C.M., 2000. Age and origin of coeval TTG, I-S-type granites in the Famatinian belt of NW Argentina. Transactions of the Royal Society of Edinburgh, Earth Sciences 91, 151–168.

Parada, M.A., Nyström, J.O., Levi, B., 1999. Multiple sources for the Coastal Batholith of central Chile (31°–34°S): geochemical and Sr–Nd isotopic evidence and tectonics implications. Lithos 46, 505–521.

Pinotti, L., Coniglio, J., Esparza, A., D'Eramo, F., Llambías, E., 2002. Nearly circular plutons emplaced by stoping at shallow crustal levels, Cerro Áspero batholith, Sierras Pampeanas de Córdoba, Argentina. Journal of South American Earth Sciences 15, 251–265.

Pinotti, L., Tubía, J.M., D'Eramo, F., Vegas, N., Sato, A.M., Coniglio, J., Aranguren, A., 2006. Structural interplay between plutons during the construction of a batholith (Cerro Aspero batholith, Sierras de Córdoba, Argentina). Journal of Structural Geology 28, 834–849.

Pitcher, W.S., 1979. The nature, ascent and emplacement of granitic magmas. Journal of the Geological Society of London 136, 627–662.

Rapela, C.W., 2000. Discusión sobre el ambiente geotectónico del Ordovícico de la región del Famatina. Revista de la Asociación Geológica Argentina 55, 134–138.

Rapela, C.W., Toselli, A., Heaman, L., Saavedra, J., 1990. Granite plutonism of the Sierras Pampeanas: an inner cordilleran Paleozoic arc in the Southern Andes. In: Kay, S.M., Rapela, C.W. (Eds.), Plutonism from Antarctica to Alaska: Geological Society of America, Special Paper, 241, pp. 77–90.

Rapela, C.W., Pankhurst, R.J., Dahlquist, J.A., Baldo, E.G., Casquet, C., Galindo, C., 2008a. Revisiting accretionary history and magma sources in the Southern Andes: time variation of "typical Andean granites". International Symposium on Andean Geodynamics, 7th, Nice, France, extended abstracts, pp. 427–430.

Rapela, C.W., Baldo, E.G., Pankhurst, R.J., Fanning, C.M., 2008b. The Devonian Achala batholith in the Sierras Pampeanas: F-rich aluminous A-type granites. San Carlos de Bariloche, Argentina South American Symposium on Isotope Geology, 6th, CD-ROM, Extended Abstract 53.

Reimann, C.R., Bahlburg, H., Kooijman, E., Berndt, J., Gerdes, A., Carlotto, V., Lopez, S., 2010. Geodynamic evolution of the early Paleozoic Western Gondwana margin 14°–17° S reflected by the detritus of the Devonian and Ordovician basins of southern Peru and northern Bolivia. Gondwana Research 18, 370–384.

Saavedra, J., Toselli, A., Rossi, J., Pellitero, E., Durand, F., 1998. The Early Palaeozoic magmatic record of the Famatina System: a review. In: Pankhurst, R.J., Rapela, C.W. (Eds.), The Proto-Andean Margin of Gondwana: Journal of the Geological Society of London, Special Publication, 142, pp. 283–295.

Scherer, E., Whitehouse, M.J., Münker, C., 2007. Zircon as a monitor of crustal growth. Elements 3, 19–24.

Siebel, W., Chen, F., 2010. Zircon Hf isotope perspective on the origin of granitic rocks from eastern Bavaria, SW Bohemian Massif. International Journal of Earth Sciences 99, 993–1005.

Siegesmund, S., Steenken, A., López de Luchi, M.G., Wemmer, K., Hoffmann, A., Mosch, S., 2004. The Las Chacras–Potrerillos batholith (Pampean Ranges, Argentina): structural evidence, emplacement and timing of the intrusion. International Journal Earth Sciences 93, 23–43.

Sims, J.P., Ireland, T.R., Camacho, A., Lyons, P., Pieters, P.E., Skirrow, R.G., Stuart-Smith, P.G., 1998. U–Pb, Th–Pb and Ar–Ar geochronology from the southern Sierras Pampeanas, Argentina: implications for the Palaeozoic tectonic evolution of the western Gondwana margin. In: Pankhurst, R.J., Rapela, C.W. (Eds.), The Proto-Andean Margin of Gondwana: Geological Society, London, Special Publications, 142, pp. 259–281.

Söderlund, U., Patchett, P.J., Vervoort, J.D., Isachsen, C.E., 2004. The ^{176}Lu decay constant determined by Lu-Hf and U–Pb isotope systematics of Precambrian mafic intrusions. Earth and Planetary Science Letters 219, 311–324.

Spagnuolo, C.M., Rapalini, A.E., Astini, R.A., 2012. Assembly of Pampia to the SW Gondwana margin: a case of strike–slip docking? Gondwana Research 21, 406–421.

Steiger, R.H., Jäger, E., 1977. Subcommission of geochronology: convention on the use of decay constants in geo- and cosmochronology. Earth and Planetary Science Letters 36, 359–362.

Stuart-Smith, P.G., Miró, R., Sims, J.P., Pieters, P.E., Lyons, P., Camacho, A., Skirrow, R.G., Black, L.P., 1999. Uranium–lead dating of felsic magmatic cycles in the southern Sierras Pampeanas, Argentina: implications for the tectonic development of the proto-Andean Gondwana margin. In: Ramos, V.A., Keppie, J.D. (Eds.), Laurentia Gondwana connections before Pangea: Geological Society of America Special Publication, 336, pp. 87–114.

Tohver, E., Cawood, P.A., Rossello, E.A., Jourdan, F., 2012. Closure of the Clymene Ocean and formation of West Gondwana in the Cambrian: evidence from the Sierras Australes of the southernmost Rio de la Plata craton, Argentina. Gondwana Research 21, 394–405.

Vaughan, A.P.M., Pankhurst, R.J., 2008. Tectonic overview of the West Gondwana margin. Gondwana Research 13, 150–162.

Vervoort, J.D., Blichert-Toft, J., 1999. Evolution of the depleted mantle: Hf isotope evidence from juvenile rocks through time. Geochimica et Cosmochimica Acta 63, 533–556.

Wedepohl, K.H., 1995. The composition of the continental crust. Geochimica et Cosmochimica Acta 59, 1217–1232.

Willner, A.P., Gerdes, A., Masonne, H.J., 2008. History of crustal growth and recycling at the Pacific convergent margin of South America at latitudes 29°–36° S revealed by a U–Pb and Lu–Hf isotope study of detrital zircon from late Paleozoic accretionary systems. Chemical Geology 253, 114–129.

Willner, A.P., Gerdes, A., Massonne, H.-J., Schmidt, A., Sudo, M., Thomson, S.N., Vujovich, G., 2011. The geodynamics of collision of a microplate (Chilenia) in Devonian times deduced by the pressure–temperature–time evolution within part of a collisional belt (Guarguaraz complex, W-Argentina). Contributions to Mineralogy and Petrology 162, 303–327.

Wilson, M., 1989. Igneous Petrogenesis, A Global Tectonic Approach. Unwin Hyman, London, p. 466.

Woodhead, J., Hergt, J., Shelley, M., Eggins, S., Kemp, R., 2004. Zircon Hf-isotope analysis with an excimer laser, depth profiling, ablation of complex geometries, and concomitant age estimation. Chemical Geology 209, 121–135.